Contribution of petrophysical analysis and 3D digital survey in the archaeometric investigations of the Emperor Hadrian's Baths (Tivoli, Italy)

Stefano Columbu, Fabio Sitzia & Giorgio Verdiani

Rendiconti Lincei
SCIENZE FISICHE E NATURALI

ISSN 2037-4631

Rend. Fis. Acc. Lincei
DOI 10.1007/s12210-015-0469-3

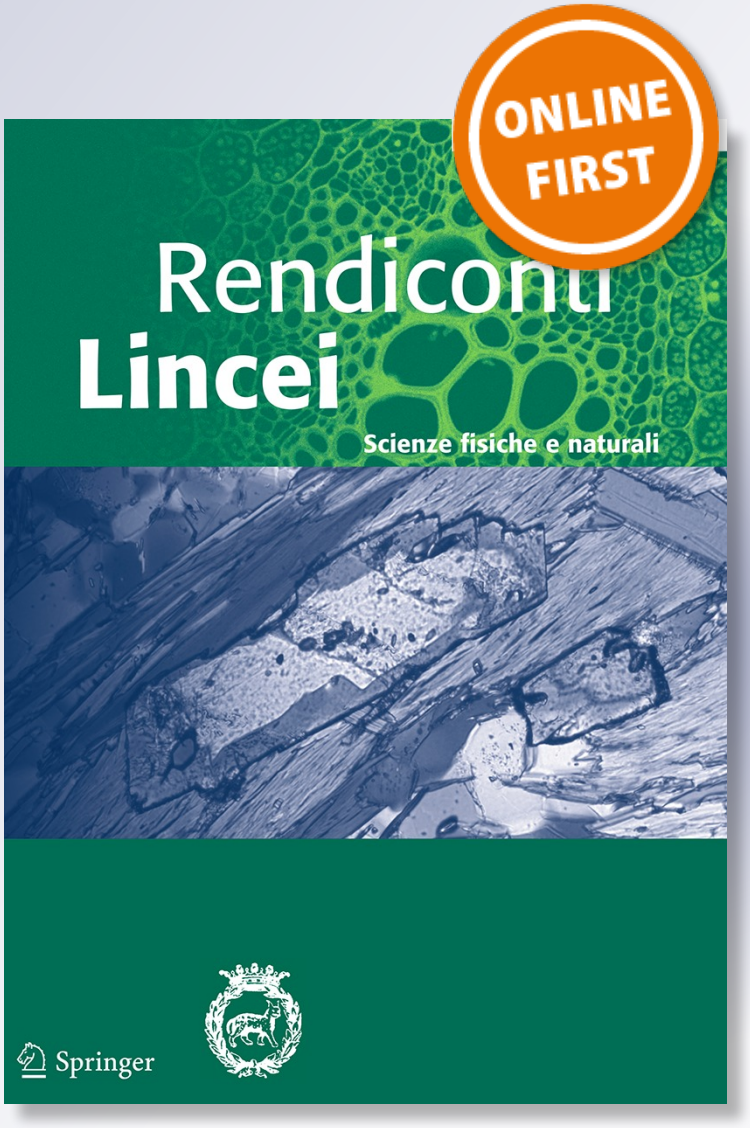

Springer

Rend. Fis. Acc. Lincei
DOI 10.1007/s12210-015-0469-3

GEOSCIENCES AND CULTURAL HERITAGE

Contribution of petrophysical analysis and 3D digital survey in the archaeometric investigations of the Emperor Hadrian's Baths (Tivoli, Italy)

Stefano Columbu[1] · **Fabio Sitzia**[1] · **Giorgio Verdiani**[2]

Received: 14 January 2015 / Accepted: 27 August 2015

Abstract This work studies the *Heliocaminus* Baths. From an architectural point of view, this is a special and unique building in the complex of the Hadrian's Villa in Tivoli. This research is carried out with a multidisciplinary approach combining petrophysical, petrographic and mineralogical characterization with the techniques of digital survey. The purpose of the research is to contribute to the understanding of Roman construction through the study of materials and from architectural aspects. Using mineral-petrographic and physical analysis, a set of samples (mortars and stones) was investigated for composition and physical properties (density, porosity, water absorption, mechanical strength, etc.). In the case of mortars, these parameters, together with the particle size distribution and the binder/aggregate ratio determined in two ways using image analysis (on thin sections and on specimens), have shown a relationship between the physical and compositional characteristics and the function of mortars within the structure of the *Heliocaminus* Baths. However, in some cases, different characteristics were detected between the mortars belonging to the same masonry and with same function in the building, showing a slight inhomogeneity in the production of mortars. Furthermore, some relationships between compositional, physical aspects (i.e. porosity, sorting and size of aggregate) and mechanical strength have been found. All the gathered data, linked to the point cloud 3D model, allowed an accurate location of the traces from the construction story of this structure.

Keywords Petrographic characterization · Physical features · Mortar · 3D Laser scanner · Roman architecture

"This contribution deals with topics considered in the session, "Archaeometry and Cultural Heritage: the contribution of Geosciences" held during the conference "The future of the Italian Geosciences, the Italian Geosciences of the future", organized by the Società Geologica Italiana and the Società Italiana di Mineralogia e Petrologia, Milano, September 10–12, 2014".

Electronic supplementary material The online version of this article (doi:10.1007/s12210-015-0469-3) contains supplementary material, which is available to authorized users.

✉ Stefano Columbu
columbus@unica.it; stefano.columbu@yahoo.it

Fabio Sitzia
fasitzia@tiscali.it

Giorgio Verdiani
giorgio.verdiani@unifi.it

[1] Dipartimento di Scienze Chimiche e Geologiche, University of Cagliari, Via Trentino 51, 09127 Cagliari, Italy

[2] Dipartimento di Architettura, University of Firenze, Florence, Italy

1 Introduction and aims

The personal baths of Emperor Hadrian (76–138 AD) are located in his villa in Tivoli (Fig. 1), a luxurious residence from the Roman Imperial Age (MacDonald and Pinto 2006). The construction of the villa began in 118 AD, just a few years after his proclamation. The practice of owning a marvellous residence outside Rome became typical for the Roman emperors starting from Tiberio (42 BC–37 AD) and the Hadrian's Villa follows this in a specific way, being not only an imperial residence but also a place for arts and architectural experimentations (Salza Prina Ricotti 2000). The construction continued almost without stops for 20 years until Hadrian's death. The complex of the villa, even if not completed, was used by Hadrian's successors. Over time the villa was a laboratory for architectural creativity, where technological and

Published online: 22 September 2015

Fig. 1 Photo-overview of the 3D model of Hadrian's Villa (made by Italo Gismondi, 1956), where the *Heliocaminus* bath is highlighted (on the *central left*)

architectural innovations were experimented to create an environment characterized by advanced urban and technical solutions (Camiz 2004), with the use of various kinds of geomaterials (Lapuente et al. 2012).

In this paper, we analyse the baths of Hadrian in one of the most innovative buildings inside the villa, called *Heliocaminus* Baths (Fig. 2). The presence of the *Heliocaminus* room, characterized by a dome-shaped coverage and by various technical solutions, underlines the importance of this construction (Verduchi 1975; Cicerchia 1985). This original architectural characteristic is probably due to the Hadrian interest about architecture, showing a particular fondness for the dome structures. The construction of these baths, as well as of the villa, is linked to different phases, often in relation with the travels of the emperor along the empire boundaries.

To study and understand the construction stages used in these complex structures, the investigations must be addressed in a multidisciplinary way, with different operating phases, from the geometric survey of the structure, to the formal analysis of architectural styles, to the study of wall textures, taking samples to directly analyse the materials, from mortars to raw materials to finishing stones, i.e. marbles (Antonelli et al. 2013; Attanasio et al. 2009, 2013; Columbu et al. 2014a; Pensabene et al. 2012; Salvatori et al. 1988). Therefore, there is often an overlap of technical–scientific, architectural and archaeological activities, but all of them are aimed at understanding the cultural significance of the artefact in its historical, artistic and political context. Among these various disciplines, an important role in the archaeometric studies of cultural heritage is assumed by applied petrography and laser scanner technologies (Antonelli et al. 2014; Bertorino et al. 2002; Columbu and Verdiani 2011, 2014; Columbu et al. 2013; Crisci et al. 2002; De Luca et al. 2013; Maravelaki-Kalaitzaki et al. 2003; Lezzerini et al. 2014; Miriello et al. 2010, 2015; Verdiani and Columbu 2010; Vola et al. 2011). The former, over a basic characterization of the rocks addressed to analyse relations between their petrographic and physical characteristics (Columbu et al. 2015), provide a focused study of technical properties and quality of geomaterials. The knowledge and basic skills are needed to address specific historical or archaeological issues (e.g. provenance and trade routes of geomaterials, construction technology in different historical periods) or conservative problems (e.g. analysis of the causes of weathering, techniques of preservation, protection and restoration).

The main aim of this work is to recognize and study the construction materials (mortars and stones) through the minero-petrographic and petrophysical characterization and 3D digital survey of the existing structure of the *Heliocaminus* Baths.

The petrographic study can provide significant data about: (1) preparation methods of mortars and different mixing ratios of binder/aggregate, with the help of image analysis on thin sections and on specimen faces of mortar bulk sample; (2) compositional characteristics and geological provenance of geomaterials used for *cubilia* (small ashlars with truncated pyramidal shape and square base used to construct the walls) or as aggregate in the mortars (e.g. volcanic scoria, leucitites). These latter, linked to the function performed by the mortar in the structure, indirectly reflect the uses and selection of raw materials. Furthermore, the analysis of some important physical properties (density, porosity, water absorption and saturation, mechanical strength, etc.) allows us to verify the built quality, testified by the proper use of geomaterials in the mortars or in the structure. In this work, to understand the different incidence of the components, the physical properties were determined, not only on bulk samples of mortar, but also on the binders and main types of aggregate (volcanic and lateritious).

The digital survey through 3D laser scanning not only provides an accurate picture of the space useful for reading the functions of the baths (Columbu and Verdiani 2011), but also allows a three-dimensional view of the wall textures used for the construction, showing the exact position of the analysed geomaterials. The obtained petrographic and physical data can then be associated as a digital database connected to the three-dimensional graphic representation of the monument.

2 Materials and methods

In the construction of the *Heliocaminus* Baths, various materials were used, some of natural origin (i.e. rocks, sands, clays, etc.) and others artificial (e.g. earthenware). To make the masonry walls and the interiors, the constructors used bricks, worked stones, marble slabs (Columbu et al. 2014a) and volcanic rocks for *cubilia* ashlars taken from local outcrops. For the production of mortars, concretes and artificial conglomerates, the aggregates used are: river and volcanic sands and pebbles, *lateritious* fragments (bricks, tiles,

Fig. 2 *Heliocaminus* Baths: **a** view from the inside of the service tunnel (Cryptoporticus); **b** view from the ground to the *Heliocaminus* vault; **c** internal view with the suspensura; **d** internal view of one of the vaults; **e** the 3D laser scanner at work in *front* of the *Heliocaminus* vault, with targets attached on the walls; **f** internal view with the large openings in the vault and one of the planar targets

pottery). In the specific case, the artificial conglomerates are distinguished from concrete, as they are composed of an aggregate of additional coarse *cocciopesto*, with sharp edges and varying grain size (from millimetric to centimetric). These conglomerates have been used in the baths for the cast (*rudus*) made for the floors and for the scratch coat (*trullisatio*) of the inner walls.

This work is oriented to study the following materials (Table ESM 1, Online Resource 1): the bedding mortars of bricks (in Latin *Opus Testaceum*; ADTH six, Fig. 3a) and *cubilia* ashlars (in Latin *Opus Reticulatum*; ADTH 23, Fig. 3b), the bedding mortars of marble coatings used for covering the floors (ADTH 37, Fig. 3c) and walls (ADTH 7, Fig. 3d), the *cocciopesto* conglomerates (in Latin *Opus Signinum*) of floors (*rudus*; ADTH 3, Fig. 3e) and walls (*trullisatio*; ADTH 25, Fig. 3f), concretes from the vaults (in Latin *Opus Caemeticium*; ADTH 53, Fig. 3g), the plasters of interior walls (ADTH 14, Fig. 3h), the volcanic rocks and the *lateritious* fragments used as aggregate in the mortars, and the volcanic stones of *cubilia* ashlars.

Fig. 3 Sampling: **a** ADTH six sample of bedding mortar of bricks taken from the *calidarium* wall (*F room* in the map of Fig. 4); **b** ADTH 23 sample of bedding mortar of *cubilia* from the *natatio* wall (*A room* in the map); **c** ADTH 37 sample of floor marble-coatings mortar from *sudatio* (*H room*); **d** ADTH 7 sample of wall marble-coating mortar taken from *sudatio*; **e** ADTH 3 sample of floor conglomerates from *calidarium*; **f** ADTH 24 sample of floor marble-coating mortar and ADTH 25 sample of floor conglomerate from *natatio*; **g** ADTH 53 sample of vault concrete from *apodyterium* (*L room*); **h** ADTH 14 sample of plaster from the *calidarium* wall (*E room*)

2.1 Operative activities

Research activities and survey investigations on the *Heliocaminus* Baths in the Hadrian's Villa are set according to the following operative phases:

- historical research, through the study of existing bibliography and unpublished archival sources;
- digital survey with 3D laser scanner technology;
- architectural reading and analysis of the structural aspects (planimetric distribution, building systems, wall textures, etc.);
- mapping of macroscopic characteristics of materials;
- sampling of materials from the baths as a function of the representativeness of the lithotypes and mortars

used (according to recommendations Nor.Ma.L. 3/80, 1980);
- sampling of raw materials (pyroclastites) used for *cubilia* ashlars from outcrops inside the Hadrian Villa area;
- petrographic, petrophysical and physical–mechanical analysis of materials (mortars and stones).

2.2 Sampling

From the *Heliocaminus* Baths, 68 samples (Fig. 4; Table ESM 1, Online Resource 1) of materials were collected. Then, 52 samples were selected for physical and petrographic analysis: 30 mortars, 14 aggregate fragments (of which seven were volcanic scoria, three leucitites and four cocciopesto), 3 *lateritious* samples (*lateritious* 1 = ADTH2 and ADTH 41 samples from *Heliocaminus* Baths; *lateritious* 2 = ADGT 2 sample from "Grandi Terme" Baths of Hadrian Villa located near the *Heliocaminus* Baths), 3 samples of volcanic tuffs of *cubilia* ashlars and 2 samples from the volcanic tuff outcrops (probably ancient quarry) within the archaeological site of the Hadrian's Villa to identify the provenance of *cubilia* stone.

Samples of mortars and stones are taken from the superficial portions of the masonry, having maximum volumes of about 20–25 cm^3, compatibly with the limits imposed by the Superintendence of Cultural Heritage of Lazio Region, which has imposed a maximum number and quantity of samples. However, the size of the material taken from the baths is representative and suitable for determining the compositional and physical characteristics of the mortars studied.

The sampling of the representative mortars was made from structures with different functions in the *Heliocaminus* Baths, according to eight groups (Table ESM 1, Online Resource 1): three wall bedding mortars of *cubilia* (*Opus Reticulatum*), seven wall bedding mortars of bricks (*Opus Testaceum*), four floor covering bedding mortars (*Marmor pavimentum*), three wall covering bedding mortars (*harenata marmor*), five floors conglomerates with *cocciopesto* aggregate (*Opus Signinum* of *rudus*) and three wall conglomerates with *cocciopesto* aggregate (*Opus Signinum* of *trussillatio* or *rinzaffo* layers), three concretes of collapsed vaults (*Opus Caementitium*) and two plasters (*arriccio* layers). From these mortars, the aggregate fragments of *cocciopesto*, volcanic scoria and leucitites were extracted through disintegration.

The mortars with the same function were sampled according to different heights in the structure and/or in diverse environments. Then, each sample was prepared in the laboratory as: pseudo-prismatic specimen (with an average size of 15 × 15 × 15 mm) on which to determine the physical properties; specimen for thin sections with a thickness around 30 μm for the microscopic analysis; a small fragment (only for some mortar samples) from which to extract the volcanic aggregate for physical analysis. On the basis of the material availability, to better characterize

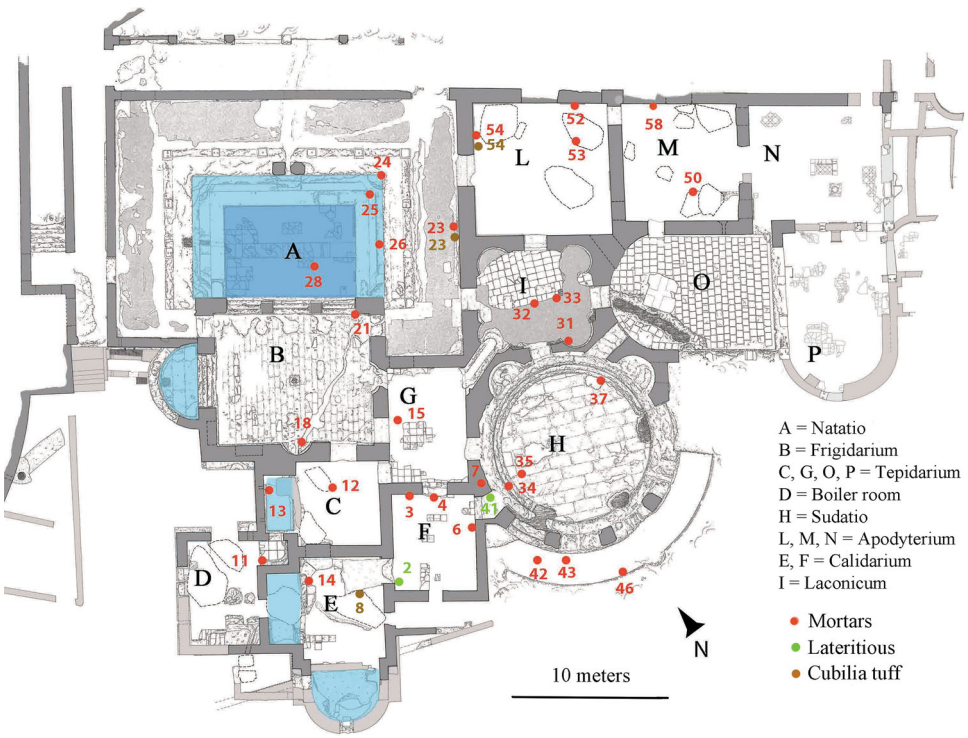

Fig. 4 Map of *Heliocaminus* Baths with sampling points of mortars and other materials

the variability of physical properties of each lateritious and tuff samples, four or five pseudo-prismatic specimens (labelled as: a, b, c, d, e) were cut and analysed.

2.3 Petrographic and petrophysical methods

Petrographic determinations of mineralogical composition were carried out by optical polarized microscopy on polished thin sections on 38 samples (30 consolidated by epoxy resin mortars, 3 *lateritious*, 5 volcanic tuff). In the case of volcanic stones, the thin sections were cut orthogonally to flow volcanic planes, whereas those of the mortars were cut perpendicularly to the outer surface of the samples. Modal analysis of mortars has been determined with "points counter" on about 300 points for each thin section.

The binder/aggregate ratio (B/A) of mortars was calculated through image analysis (by ImageJ 1.47v) in two different ways: (1) on photographs taken on six faces of the cubic specimens of mortars on which the physical–mechanical tests have been determined; (2) on thin section photographs detected with the flatbed scanner.

The physical tests were determined on 82 cubic specimens extracted from unaltered portion of samples after removing the exterior part of the mortar. The specimens were dried at 105 ± 5 °C and the dry solid mass (m_D) was determined. The solid phase volume (V_S) of powdered rock specimens (on 5–8 g and with particle size less than 0.063 mm) and the real volume (with $V_R = V_S + V_C$, where V_C is the volume of pores closed to helium) of the specimens were determined by helium Ultrapycnometer 1000 (Quantachrome Instruments). Then, the wet solid mass (m_W) of the samples was determined after water absorption by immersion for 10 days. Through a hydrostatic analytical balance, the bulk volume V_B (with $V_B = V_S + V_O + V_C$, where $V_O = (V_B – V_R)$ is the volume of open pores to helium) is calculated as:

$$V_B = [(m_W - m_{HY})/\rho_w T_{25\,^\circ C}] \times 100,$$

where m_{HY} is the hydrostatic mass of the wet specimen and $\rho_W T_{25\,^\circ C}$ is the water density at a temperature of 25 °C.

Total porosity (Φ_T), open porosity to water and helium ($\Phi_O H_2O$, $\Phi_O He$, respectively), closed porosity to water and helium ($\Phi_C H_2O$; $\Phi_C He$), bulk density (ρ_B), real density (ρ_R)and solid density (ρ_S) were computed as:

$$\Phi_T = [(V_B - V_S)/V_B] \times 100,$$

$$\Phi_O H_2O = [(m_W - m_D)/m_W T_X]/V_B \times 100,$$

$$\Phi_O He = [(V_B - V_R)/V_B] \times 100,$$

$$\Phi_C H_2O = \Phi_T - \Phi_O H_2O\ ,$$

$$\Phi_C He = \Phi_T - \Phi_O He.$$

$\rho_S = m_D/V_S$; $\rho_R = m_D/V_R$; $\rho_B = m_D/V_B$.

The weight imbibition coefficient (IC_W) and the saturation index (SI) were computed as:

$$IC_W = [(m_W - m_D)/m_D] \times 100,$$

$$SI = (\Phi_O H_2O/\Phi_O He) = [(m_W - m_D)/\rho_W T_X]/V_O \times 100.$$

The punching strength index was determined with a Point Load Tester (mod. D550 Controls Instrument) according to the ISRM (1972, 1985) on the same pseudo-cubic rock specimens used for other physical properties (Table ESM 1, Online Resource 1). The load was exerted via the application of a concentrated load with two opposing conical punches. The resistance to puncturing (I_S) was calculated as P/D_e^2, where P is the breaking load and D_e is the "equivalent diameter of the carrot" (ISRM 1985), with $D_e = 4A/\pi$ and $A = W \times D$, where W and 2L are the width perpendicular to the direction of the load and the length of the specimen, respectively. The index value is referred to a standard cylindrical specimen with diameter $D = 50$ mm for which I_S has been corrected with a shape coefficient (F) and calculated as:

$$I_{S(50)} = I_S \times F = I_S \times (D_e/50)^{0.45}.$$

The simple compression resistance (R_C) and the traction resistance (R_T) of the mortar were indirectly calculated (according to ISRM 1985) using the value of normalized punching resistance, with each of them as:

$$R_c = K \times I_{s(50)},$$

$$R_T = I_{s(50)}/0.8,$$

where K (multiplication coefficient) = 14 (Palmström 1995).

To proceed with the particle-size analysis, the mortars were first disaggregated with the use of a mortar and pestle, dried at 105 ± 5 °C, weighed to measure the dry mass (m_{dM}) and then reacted with acid solution (HNO_3, 13 % vol.) for a period of immersion of 48 h, so as to eliminate the carbonate binder matrix of the mortar. The samples were then filtered with Whatman 41 paper, washed in distilled water, placed in an oven at 105 ± 5 °C to determine the dry mass of the residual aggregate (m_{dR}) and, indirectly, the bulk mass of the binder (as: $m_{dB} = m_{dM} - m_{dR}$). Then, the particle-size distribution was performed using sieves series UNI 2131, with mesh opening of 4000, 2000, 500, 250, 125 and 63 μm with sifter Giuliani IG3.

2.4 Laser scanning survey

The whole digital survey was done using a 3D laser scanner unit supported by a Leica Geosystem TP-706

topographical total station; the long time research inside the Hadrian's Villa (carried on by the Florentine "Dipartimento di Architettura" from 2004 to 2011) was based on a main topographical network. In this way, it was possible to easily reconnect each new digital survey campaign to the previous, creating a progressive extension of the covered area in a unique reference system. The matching between the 3D scans and the topographical network was materialized placing specific targets in place, and this set of graphical elements was measured both by the total station and by the 3D laser scanner. The scanner used in the survey of the *Heliocaminus* Baths was a Cam2 Faro Photon, with phase shift-measuring technology (see Fig. 2e). This allowed a high level of detail in a quite wide operative range (from 1 to 40 m in the *Heliocaminus* survey) and made a very quick operating time possible, allowing to cover extended parts of the monument in a few hours. The quite versatile structure of this scanner was also useful for the positioning and the setting of each scan station, allowing to climb on ruins and wall and/or to rise the scanner to the heights needed to reach most of the top parts of the building. The positioning of the scan stations was decided according to the shape and to the specific conditions of each space. The survey was completed taking 110 scan stations, all of them made in full panoramic mode, exploiting the characteristics of the 3D laser scanner in use, which was capable of scanning 360° on the vertical axis and 320° on the horizontal one. The scanning was conducted in two separated sequences: a first round turn all around the monument area, placing the scanner at the maximal possible distance (the *Heliocaminus* Baths has a lot of structures in its nearby area), and often over walls to reach a good elevation and reduce the residual occlusion spaces in the top parts of the building. A second sequence of scans was done for the internal parts; this second sequence can be divided into two complementary groups, the one dedicated to the "rooms" (i.e. *calidarium*, *tepidarium*, changing rooms, bathrooms, internal pools, etc.) and the one dedicated to the "technical spaces" (i.e. *suspensura*, furnaces, hot air tunnels, service tunnels, etc.). The scanning of the inner parts has required particular attention to avoid any possible occlusion space.

A monumental ruin like this one is more complex to be completely covered then a well-preserved building or an excavated site. The altered shape of the walls and the "organic" form assumed by walls, vaults and openings need attention and cure in creating a full coverage without overmeasuring large areas of the buildings. In this, the support of a topographical network is very useful, while it reduces the need for overlapping scans and allows to concentrate on the reduction of occlusion spaces. Each room received an adequate number of scans, aimed at having no "holes" (or at least, no significant ones) in the final model. The connection between each scan and the topographical network was "materialized" in a system of specific targets, temporarily put in place for the time of the survey. Two systems of targets were used: planar ones (classical black and white checkerboard models, square shaped, made of cardboard) measured both by the scanner and by the topographic unit (see Fig. 2e); and spherical ones (10–20 cm diameter, made of white polystyrene foam) measured only by the 3D laser scanner and used for an even more reliable connection of the internal and external scans. Each scan was operated obtaining a grid around 1 × 1 cm over the main subject of each scan (a wall, a couple or a group of walls, a ceiling, the central part of a vault), but because each room needs more than a single scan to be completely documented, the final grid is more dense than this. The overall survey work was characterized by an accuracy around 2–5 mm, which is more than a satisfactory value for the final 5 × 5, 6 × 6 mm final grid obtained for most of the surfaces of this building. All the scanning work was later aligned over the topographical network, combining all the point clouds together to show a global digital model made of vector points capable of describing in detail the whole monument. The process of alignment, commonly called "registration", was a quite quick operation and it was done using the Leica Geosystem Cyclone software. In this way, it was possible to control with a great accuracy the quality of the general alignment. At the same time, the solid topographical network gave the opportunity to combine the *Heliocaminus* Baths in the large overall system of the villa, together with the large baths, the small baths, the *Serapeo*, the *Cento Camerelle* and all other areas taken in the years of survey work inside Hadrian's Villa.

3 Results

3.1 Mortars and lateritious

3.1.1 Minero-petrographic analysis

By macroscopic observations and microscopic modal analysis in thin section, the following characteristics of mortars were defined: aggregate composition (Table ESM 2, Online Resource 2), binder reactivity with aggregate and presence of lime lumps.

The binder has colours ranging from light grey to whitish on freshly cut mortar specimens, while on the surfaces exposed to the outside, due to the weathering, in some cases the samples show more intense colours up to grey. There is frequent presence of lumps with dimensions from sub-millimetre to 6 mm (Columbu and Verdiani 2011).

Biological patinas are often present with a colour from grey-black (e.g. moulds) to light green to white to yellow (e.g. mosses, lichens).

The aggregate is composed of volcanic rock clasts (as natural gravel), crystal clasts (i.e. single crystalline phases), *cocciopesto* fragments (crushed bricks, tiles, pottery, mainly in the wall and floor conglomerates) and rare fragments of marbles (Table ESM 2, Online Resource 2).

The volcanic aggregate is composed of leucitic basalt (represented mainly by scoria clasts) and leucitite belonging to the alkaline rocks of ultrapotassic series (HKS) of the Roman Magmatic Province (Morbidelli 2003; Peccerillo 2005).

The aggregate of leucitic basalt (Fig. 5a, b) that is present in all mortars with greater frequency (>70 % of total aggregate; Table ESM 2, Online Resource 2) shows great similarity with the volcanic scoria outcropping in several points around the area of the Hadrian's Villa. This aggregate has predominantly sub-spherical shapes and a colour from grey-red or grey-black.

The leucitic basalt appears vitreous and porous, with afiric texture. The paragenesis is composed of clinopyroxene (Fig. 5a), leucite, green hornblende, opaque minerals (with circular shape, probably magnetite or Ti-magnetite) and rare plagioclase, all immersed into a glassy matrix. Rare crystals of biotite and olivine (this latter often altered in iddingsite) are present. The leucitic basalt aggregate shows the edges of pozzolanic reaction with the binder (Fig. 5d–f).

The aggregate of leucitite (Fig. 5c) has a frequency <8 % of total aggregate (Table ESM 2, Online Resource 2), much lower with respect to volcanic scoria. It has a greyish colouration, shape generally subspherical, low porosity and is frequently altered. The paragenesis consists essentially of leucite, clinopyroxenes and opaque minerals. The feldspars are absent or rare.

The aggregate of crystal clasts are represented by green hornblende, clinopyroxene and rare biotite.

The *cocciopesto* aggregate of mortars and *lateritious* samples (Fig. 5f, g; Tables ESM 1 and 2, Online Resources 1 and 2) shows a variable colour from yellow-ochre to pink-orange to rust-red. Immersed in the micrometric matrix, crystal clasts of quartz and plagioclase are present. Rarely, even fragments of leucitic basalts (about 3 % on the total of thin section) are found. Phases of iron oxides (i.e. haematite) are also present. The fragments of this aggregate often have angular shape with variable physical characteristics (porosity, size, etc.) and compositions. It shows clear edges of reaction with the binder (Fig. 5f, g).

The marble aggregate (Fig. 5h) is found only in small percentages in the finishing mortars (plasters), where, due to its white colour, it does not stand out chromatically on the surfaces rendered white by the lime (Binda and Baronio 1986). Subordinately, the marble is present also in the bedding of *cubilia* and bricks and in the concrete of the vaults. This type of aggregate has sharp edges with a microcrystalline structure of calcite crystals and opaque minerals.

3.1.2 Aggregate particle size of mortars

The results of particle-size analysis of aggregate are reported in Table ESM 3 (Online Resource 3).

Observing Fig. 6a, except for some cases, the samples show a selected aggregate, frequently with modal classes in 4000 and 2000 μm and with a progressive decrease of hold mass % to lower size in the other classes.

The bedding mortars of brick have a modal class of 4000 μm (with range 35–61 % of hold mass; Table ESM 3, Online Resource 3), with the exception for the samples ADTH 4 and ADTH 42 (Fig. 6b), characterized by modal classes of 1000 and 2000 μm, respectively. For these samples, different grain size of the aggregate was selected, because there are bedding mortars of the *lateritious* tiles from the floors of the *calidarium* (F room in the map of Fig. 4) and from the circular room located around the *sudatio* room with *Heliocaminus*.

The bedding mortars of *cubilia* have a distribution similar to those of brick bedding mortars, but show a greater variability of hold mass % in the classes 4000 and 2000 μm.

The wall and floor coating bedding mortars have similar grain size distribution of aggregate, with low sorting and modal class around 4000 μm (with hold masses between 11 and 34 %; Table ESM 3, Online Resource 3), except the samples ADTH 28 and ADTH 37 of marble-coating mortars belonging to the floor of *natatio* pool and the *sudatio* room, respectively, that have different distributions and more similar to the samples ADTH 4 and ADTH 42 (Fig. 6b).

The floor and wall conglomerates with *cocciopesto* have a modal class in 4000 μm, but with greater values of hold mass % (ranges 57–70 %, 34–59 %, respectively) with respect to all mortars.

The mortars representative of vault concretes are characterized by modal class of 2000 μm (samples ADTH 12 and ADTH 50; Fig. 6a) and 4000 μm (sample ADTH 53; Fig. 6b). Considering the function of these mortars, they have low values of hold mass (23–32 %) in the class 4000 μm, but the samples analysed obviously did not include the coarse aggregate and *caementia* used in the concrete casting.

The *arriccio* layers of plasters (samples ADTH 13 and ADTH 14) have a particle-size distribution (Fig. 6a) more similar to the *rinzaffo* layers (*trullisatio*) of wall conglomerates.

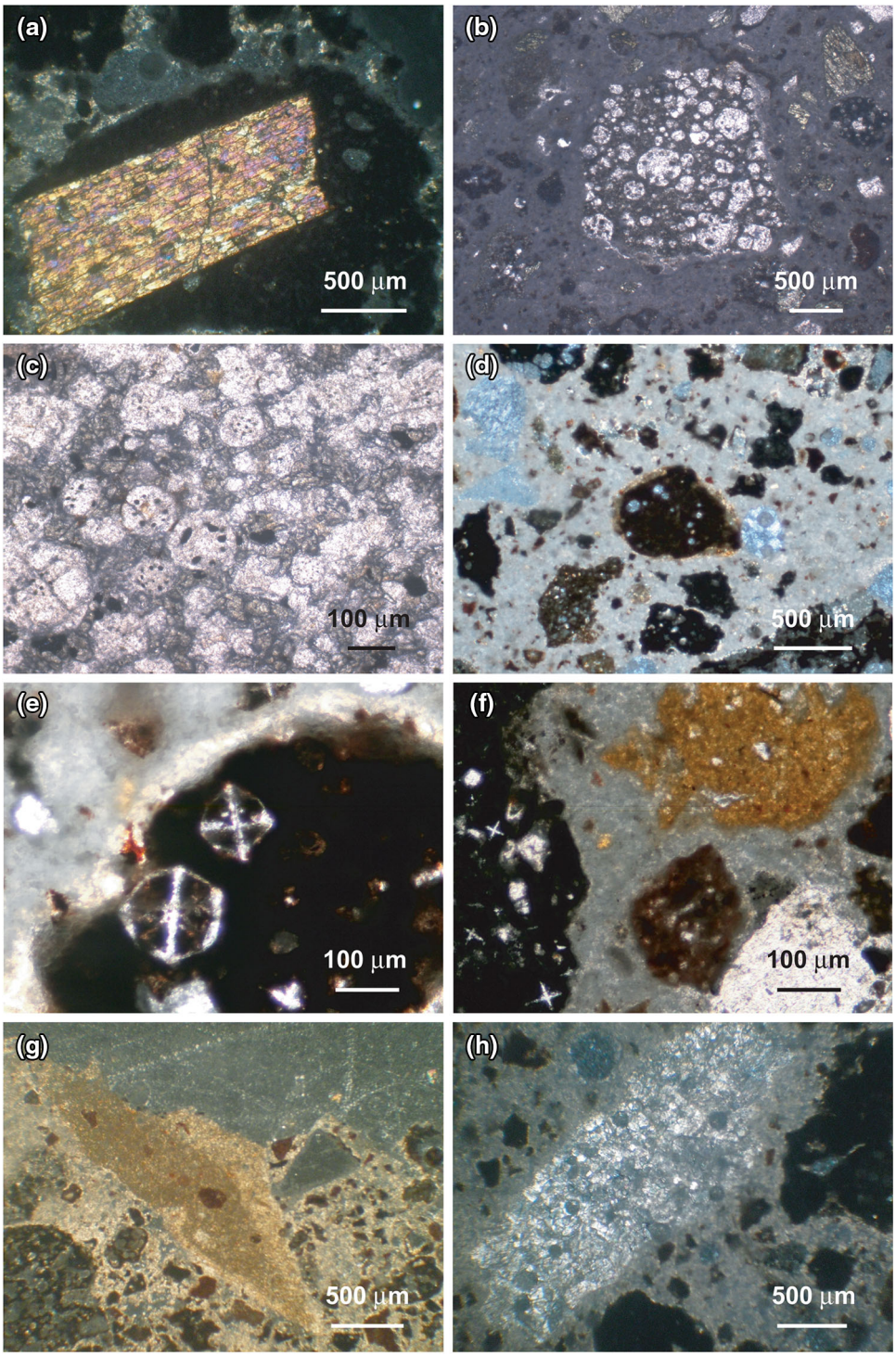

Fig. 5 Micro-photographs of mortar aggregates: **a** cross Nicol: crystal clast of clinopyroxene in the leucitic basalt; **b** plain polars: leucite crystal in the leucitic basalt; **c** plain polars: leucite crystals in the leucitites; **d** plain polars: vesicular black scoria with reaction border with binder; **e** plain polars: vesicular black scoria (inside which there are two leucite crystals) with obvious reaction border with binder; **f** plain polars: black and red volcanic scoria and *cocciopesto* aggregate; **g** plain polars: *cocciopesto* aggregate with obvious reaction border with binder; **h** cross polars: marble fragment in mortar binder

3.1.3 Binder/aggregate ratio (B/A) and function of mortars

The average values of B/A ratio, calculated through image analysis on six faces of the cubic specimens (Table ESM 4, Online Resource 4), depends on the function of mortar in the baths; they are higher in wall *cocciopesto* conglomerates (*trullisatio*) (0.70) and in the bedding mortars of bricks (0.68), while the concrete of vaults have lower values (0.54). The bedding mortars of *cubilia* and floor *cocciopesto* conglomerates (*rudus*) have intermediate values of ratio (0.62, 0.59, respectively). Except for the mortars of the concretes of the vaults, this ratio varies, however, also within the single populations of samples, highlighting a light unevenness in the preparation of mortars.

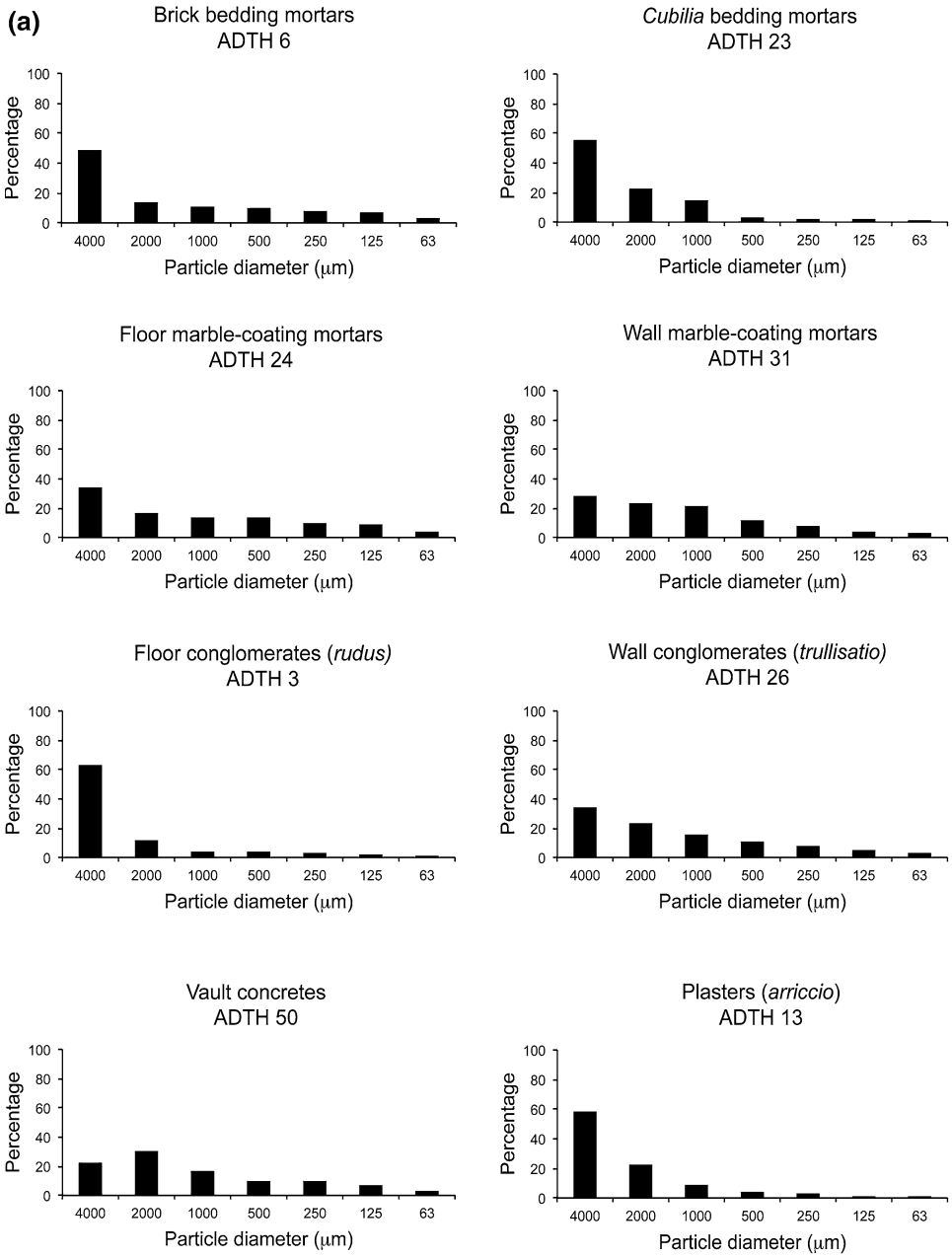

Fig. 6 Particle-size distribution of mortar aggregates in the classes 4000, 2000, 1000, 500, 250, 125 and 63 μm, where the histograms of representative samples of each mortar group with different function in the *Heliocaminus* Baths is also reported

The B/A ratios were obtained also through image analysis on microphotographs. In this latter case, the values are always higher than those obtained by image analysis on cubic specimens (Table ESM 4, Online Resource 4). This discrepancy is mainly due to the different volumes of samples analysed in the two cases.

In any case, the absolute values are higher than the values indicated by Roman architect *Vitruvio* (Pollione 15 BC), who said that: the percentage of aggregate to be used in a mortar is a function of several parameters, among which are the particle-size distribution and the thickness of the mortar cast. On the basis of these parameters, a thickness of 1–2 cm provides a percentage of the aggregate between 65 and 70 vol. %. Thickness >2 cm instead provides percentages of aggregate in the order of 70–80 vol. % (Binda and Baronio 1986). Based on the results obtained with both methods, the percentage of aggregate more similar to the recommendations of *Vitruvio* is the one obtained by image analysis on cubic specimens, although the percentage of aggregate used is always higher than the indications of the Roman architect (Collepardi 1993). Secondly, the values of the ratio B/A may be higher than those recommended due to image analysis that does not detect the presence of aggregate with very small size (<100 microns).

Fig. 6 continued

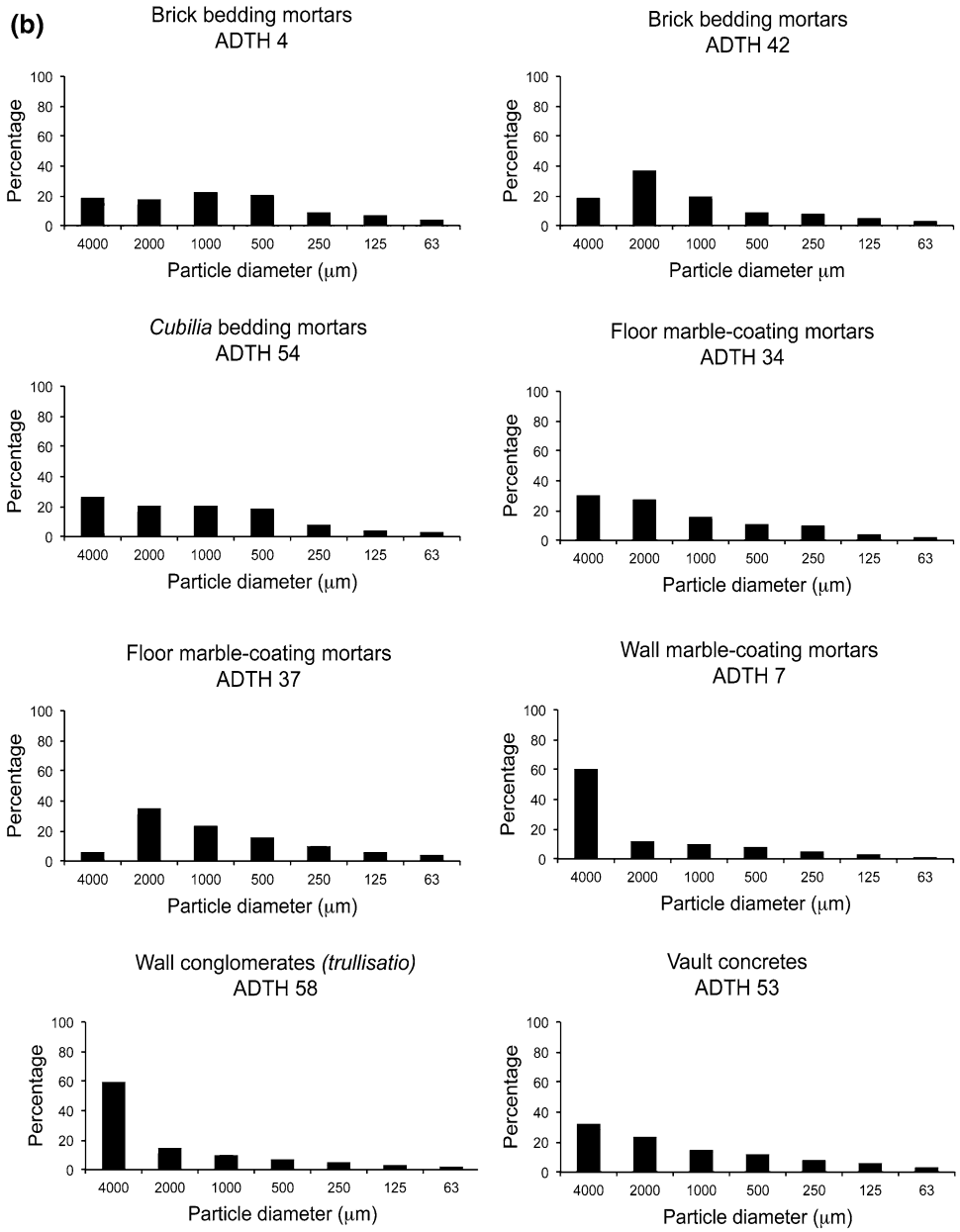

3.1.4 Physical properties

For the mortars, the following physical and mechanical properties were determined: solid, real and bulk density, open and closed porosity of helium and water, weight imbibition coefficient, saturation index and punching strength (Table ESM 5, Online Resource 5). Then, the physical analysis was made even on binder (Table ESM 6, Online Resource 6), aggregate extracts from the same mortars, volcanic scoria, leucitites (Table ESM 7, Online Resource 7), *lateritious* fragments of bricks and other earthenware from the *Heliocaminus* Baths and "Grandi terme" Baths and on *cubilia* stones and volcanic rocks from outcrops (Table ESM 8, Online Resource 8).

Here, we will discuss more the helium open porosity and less the total porosity, because the latter was determined only on samples of aggregate and *lateritites*, while the former was detected on all samples, including those of the mortars.

Physical properties are variable (Table ESM 5, Online Resource 5), due to the different incidence of binder and aggregate components and of their dimensions in relation to the size of mortar specimens analysed. Light data dispersion is present also between the samples belonging to

the same kind of mortar that demonstrates at first glance an inhomogeneity of the material.

To define the physical behaviour between the different groups of mortars, in the graphs of Fig. 7a, the He open porosity versus bulk density, usually well correlated, is reported. The vault concretes have a high coefficient of R^2 (0.99), but the samples include only three mortars and without the centimetric and decimetric coarse aggregate component (i.e. *Caementia* of volcanic stone). The bedding mortars of marble coatings (of wall and floor together) and the bedding mortars of *cubilia* and bricks (together) show correlation coefficients with R^2 values of 0.81 and 0.56, respectively. The *cocciopesto* conglomerates (from walls and floors) have a lower value (0.31) due to the variable incidence of *lateritious* aggregate parameters (density, quantity, shape and dimension of fragments) and due to the presence of a sample (ADTH 58) with anomalous lower values of porosity (Table ESM 5, Online Resource 5). In fact, without this sample, the R^2 coefficient would be 0.69.

The variability of He open porosity and bulk density in the mortars is easily understood on observing the different characteristics of the binder and aggregate (Fig. 7b; Tables ESM 6 and 7, Online Resources 6 and 7), which show a large variability of these properties, ranging in the aggregate samples from 13.7 to 48.0 % and from 1.4 to 2.2 g/cm^3, respectively, and in the binders from 15.8 to 51.1 % and from 0.38 to 1.61 g/cm^3.

Looking inside the single populations (Fig. 7a, b; Table ESM 5, Online Resource 5), the floor conglomerates show a greater homogeneity of these two physical properties in front of the other mortars, in part resulting from a good homogeneity of the binders. Then, these mortars have greater mean values of bulk density with respect to the wall conglomerates (1.50 ± 0.07 g/cm^3 versus 1.34 ± 0.13, respectively). In the same way, the binders have values 0.77 ± 0.17 versus 1.46 ± 0.48 and 0.64 ± 0.04 g/cm^3, respectively. Considered the structural function of the floor conglomerates, it is likely that these latter have undergone

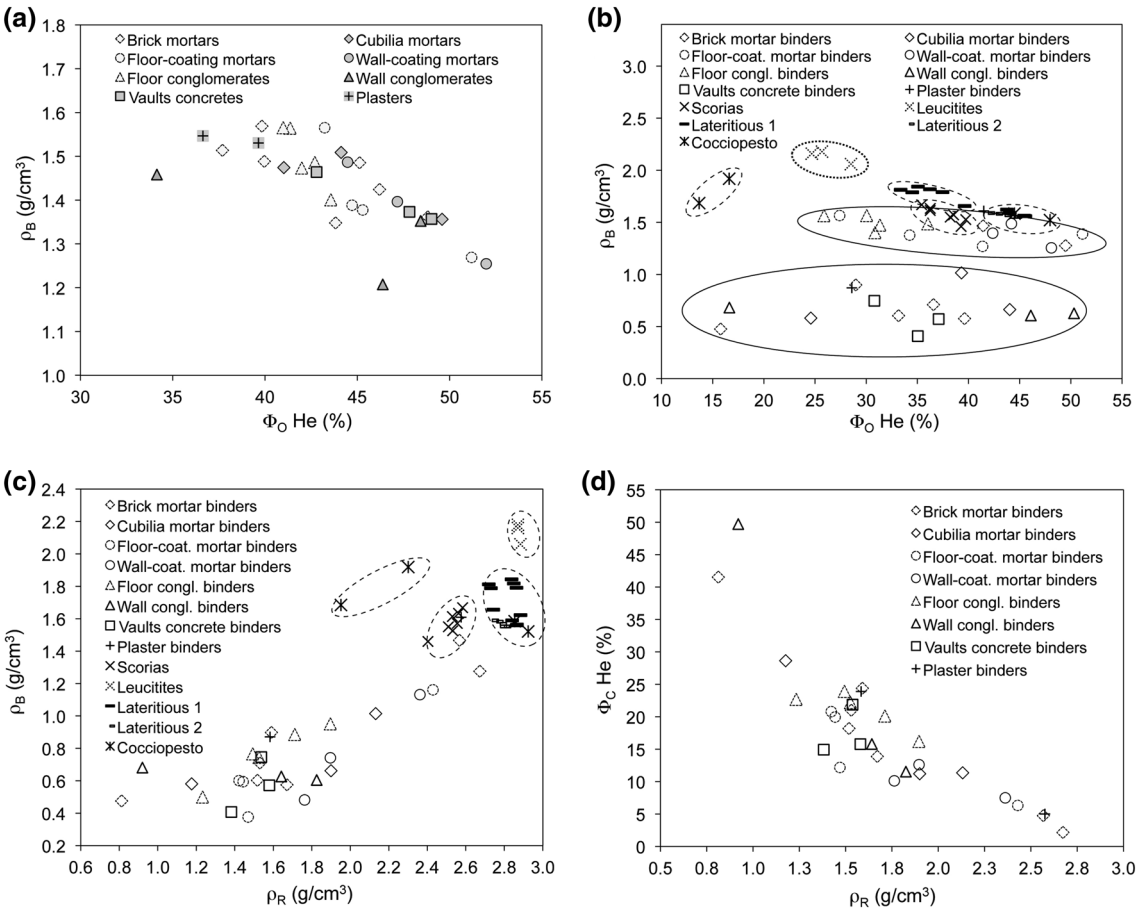

Fig. 7 Physical properties of mortars, binders and aggregates: **a** helium open porosity (Φ_OHe) versus bulk density (ρ_B) divided into eight groups of mortar typology; **b** helium open porosity (Φ_OHe) versus bulk density (ρ_B) of binders and aggregates divided into eight groups of mortar typology; **c** real density (ρ_R) versus bulk density (ρ_B) of binders and aggregates divided into eight groups of mortar typology; **d** real density (ρ_R) versus helium closed porosity (Φ_OHe) of binders divided into eight groups of mortar typology. The physical data of binders were calculated using the binder/aggregate ratios derived by image analysis determined on the pseudo-cubic specimens (Table ESM 4) and the proportions of the aggregate components defined by modal analysis of mortars in thin section (Table ESM 2)

greater compaction, due to the use of *cocciopesto* of high quality, characterized by greater real and bulk density.

The binders show also a high variability of real density (Fig. 7c, d; Table ESM 6, Online Resource 6) and closed porosity (Fig. 7d); between them exist a good exponential correlation ($R^2 = 0.85$), even if this correlation is in part related to the assumption that the solid density is constant at 2.80 g/cm^3, and so the real density is mainly influenced by the closed porosity and less by the solid density.

In the graphics of Fig. 8a, the plotted samples of mortars are positioned below the line of 100 % water saturation. Also in this case, the floor conglomerates show themselves to be more homogeneous open porosities and saturation indexes than the other mortars. In the same manner, also the binders and the samples of aggregates are below the line (Fig. 8b), but with lower values of helium open porosity, even if they probably have a total porosity (helium closed + helium open porosities) greater than the mortars. Only two samples of mortar have a binder (Fig. 8b) with a saturation index greater than 100 %, but, since they are theoretical values, a slight discrepancy is acceptable. Inside single groups of mortars, in the binders there is a high variability of porosity values.

The volcanic scoria aggregates have a saturation index close to 100 %, while the *cocciopesto* aggregates and *lateritious* fragments (bricks, tiles and crushed pottery) show lower average values of saturation index (Fig. 8b; Tables ESM 7 and 8, Online Resources 7 and 8), probably because they have a lower radius of porosities (or greater tortuosity) in front of the binders and the mortars.

In Fig. 9a, the mortars show similar values with overlap of populations and with a light correlation (well known in literature) between the mechanical resistance ($I_{S(50)}$) and helium open porosity of the mortars, indicating that the porosity in some way influences the mechanical strength. But given the low correlation coefficient ($R^2 = 0.20$; Fig. 9b) between these two properties and the small dimensions of the specimens, the factors that influence mostly the resistance are the characteristics of the binder (i.e. cohesion degree, porosity, etc.) and the particle size and shape of the aggregate. Except for the plasters, the floor conglomerates and bedding mortars have greater mechanical resistances (0.53 ± 0.26 and 0.49 ± 0.24 MPa, respectively; Table ESM 5, Online Resource 5) with respect to other mortars (range 0.25–0.28), probably due to a better quality of binder and a more resistant aggregate, as evidenced by physical data of the *lateritious* samples from *Heliocaminus* Baths (with two different populations of ADTH 41 and ADTH 2 samples; Table ESM 8, Online Resource 8; Fig. 9b) and "Grandi Terme" Baths (ADGT 2 samples). The high strength of the plasters can be explained by lower helium open porosity (38.14 ± 2.13 %; Table ESM 5, Online Resource 5) and higher bulk density (1.54 ± 0.01 g/cm^3) probably due to better mixing of the binder–aggregate.

3.2 Volcanic tuff of *cubilia* ashlars

The stone used for *cubilia* small pyramidal ashlars (with the side of the square base about 7 cm; Fig. 3b) is a pyroclastitic rock. Given its medium–low welding, it mainly shows evident physical degradation due to decohesion processes. It is characterized (Fig. 10a, b) by a glassy groundmass, occasionally with typical alterations in zeolites and clay minerals (Peccerillo 2005), where lithic clasts of varying particle size, with composition from leucitic basaltic to leucititic, and

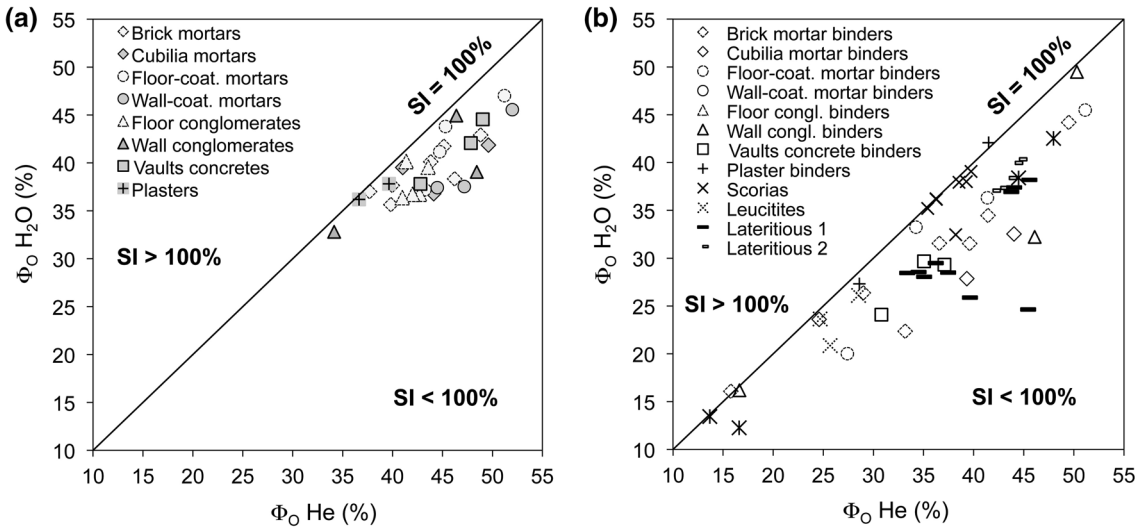

Fig. 8 Physical properties of mortars and aggregates: **a** helium open porosity (Φ_OHe) versus water open porosity ($\Phi_O H_2O$) divided into eight groups of mortar typology; **b** helium open porosity (Φ_OHe) versus water open porosity ($\Phi_O H_2O$) of binders and aggregates

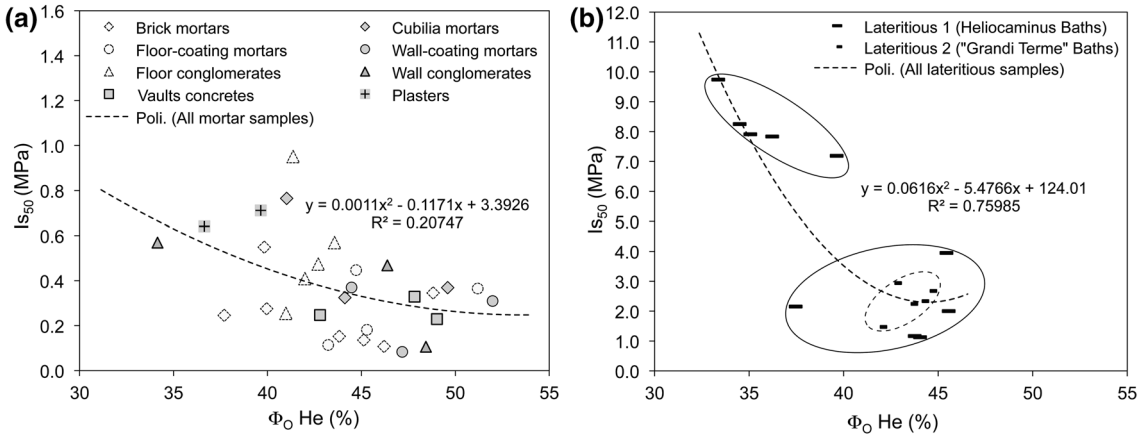

Fig. 9 Physical properties of mortars and *laterites*: **a** helium open porosity (Φ_OHe) versus point load strength index (Is_{50}) of mortars; **b** helium open porosity (Φ_OHe) versus point load strength index (Is_{50}) of *laterites*

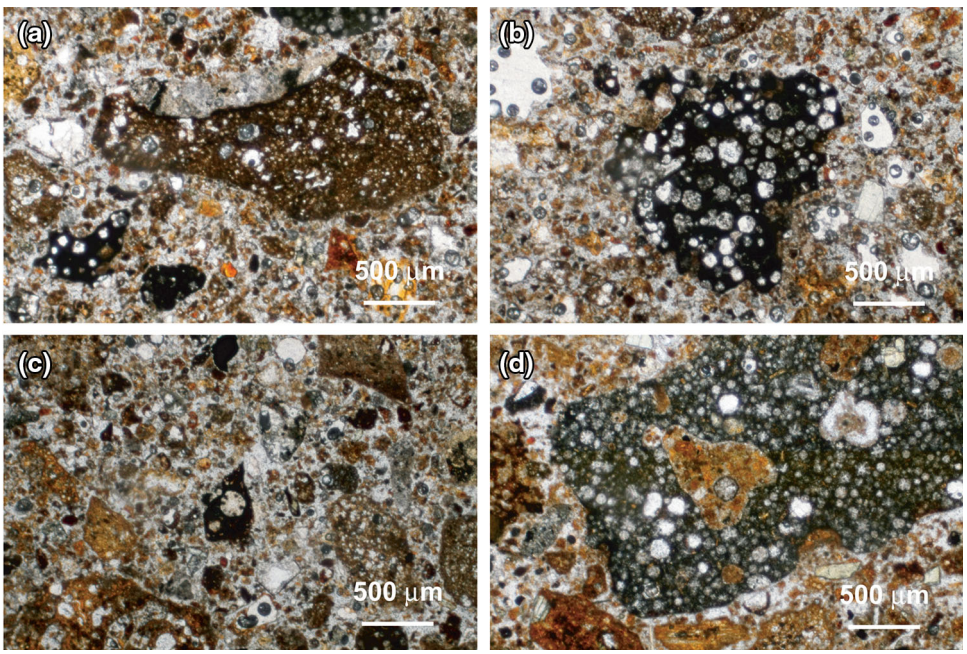

Fig. 10 Micro-photographs of *cubilia* tuff from *Heliocaminus* Baths and volcanic tuff from outcrops inside the Hadrian Villa area. **a** Plain polars: vesicular red scoria fragment inside *cubilia* stone (sample ADTH 23); **b** plain polars: black leucitite fragment inside the *cubilia* stone (sample ADTH 23); **c** plain polars: volcanic scoria and leucitite fragments on glassy groundmass of volcanic tuff belonging to outcrops (sample ADCA 1); **d** plain polars: black leucitite fragment inside volcanic tuff from outcrops (sample ADCA 2)

xenoliths are present. The accessory phases are iron and titanium oxides (Bernardi et al. 1982). By microscopic observations with parallel polars, they have a reddish-burgundy colour and only rarely grey-black.

From a comparison in thin section of volcanic tuff with samples of pyroclatites (Fig. 10c, d) collected inside the Hadrian's Villa area, it is highlighted that the volcanic material used to make the *cubilia* was in all probability extracted from outcrops near (a few hundred metres) the same baths with *Heliocaminus*.

The pyroclastites are rocks variously present in the Italian territory (e.g. Lazio, Campania, Sardinia, etc.) and due to their excellent workability and a variable physical–mechanical resistance, depending on their variable degree of welding, have been widely used in Roman and Mediaeval architecture (Columbu et al. 2014b; Melis and Columbu 2000; Macciotta et al. 2001) and as household utensils (e.g. millstones, Antonelli et al. 2014).

These materials, if containing high percentages of volcanic glass with a not too high degree of welding, were used, as in this case, also as pozzolanic aggregate in the mortars. In the specific case, it is assumed that the volcanic tuffs have been used grounded even as an aggregate in the mortars (and probably in the mixture of bricks). In fact, in the mortars the presence of the same crystal-clasts observed also in the tuff has been frequently detected (i.e. green hornblende, clinopyroxene, biotite) as well as the presence of leucitic basalt and leucitites.

In Fig. 11 the physical and mechanical data of the samples taken from *cubilia* of *Heliocaminus* Baths and from near volcanic outcrops in Hadrian's Villa area are plotted. The two populations have similar physical properties (Table ESM 8, Online Resource 8), but show different ranges of absolute values, because the samples taken from outcrops are more altered than those of the *cubilia*, as evidenced also by the different porosity, saturation index and mechanical strength of the two populations (Fig. 11a, b). A similar trend of saturation index (Fig. 11a) that decreases with the increase of He open porosity can be observed, although with different correlation coefficient R^2 (0.71 versus 0.28) due to a greater data dispersion consequently to higher alteration on the tuff from outcrops.

3.3 Digital survey and post-processing of the data

After the digital survey, once the general aligned point cloud was completed, different types of information were extracted. The first passage was aimed at the production of 2D drawings, useful in their traditional graphic, for the classical reading of the architecture and easy to be used as base for placing the collected data, applying maps and, last but not least, transferring information to others. The process of extraction of this set of drawings was a classical one: after the definition of a specific reference plane, the general point cloud was sectioned to realize horizontal and vertical sections, produced at the same scale with the points in different colour treatments. The points coloured according to their reflectance value, their distances from the reference plane, in fake colours and in greyscale, and with a special rendering graphic like "silhouette" (an enhancement of the main borders, with the hiding of the points belonging to planes with an orthogonal position in front of the viewing axis) have created a multi-level image, ready to go inside a CAD software. Using Autodesk Autocad, these images were redrawn, swapping from one to the other to have an easier reading and interpretation of the most complex parts and creating the final set of vector graphic from the original point cloud.

At the same time, a specific version of the 3D point cloud was completed and prepared, with the optimization of the data from the main building, removing its surrounding structures (Fig. 12). Then, the final point cloud was divided into separate layers, containing the parts describing the interiors and the exteriors. This structured model was the right base to receive extra information and to be the reference system to put all the collected data in a 3D space.

4 Discussion of results

4.1 Petrophysical characterization of materials

The minero-petrographic characteristics (e.g. aggregate composition, binder/aggregate ratio, textural and microstructural aspects) and physical properties of the bulk mortar samples and aggregates (density, porosity, mechanical strength, particle size, etc.) taken from the *Heliocaminus* Baths gave a significant help in understanding the method of preparation of the mortars, the proportions of aggregate components and the characteristics and provenance of the raw stone materials used in the mixture.

The mortars consist of an aggregate of various compositions (Table ESM 2, Online Resource 2) represented by black or red volcanic *scoria*, leucitites, crystal clasts, *cocciopesto* and rare marble fragments. They have different physical properties and binder/aggregate ratios, related to their function in the building (Tables ESM 3–7, Online Resources 3–7; Figs. 7, 8, 9, 11)

The mortars used for the plasters (*arriccio* and *rinzaffo* layers) and for the wall marble coatings, considering their

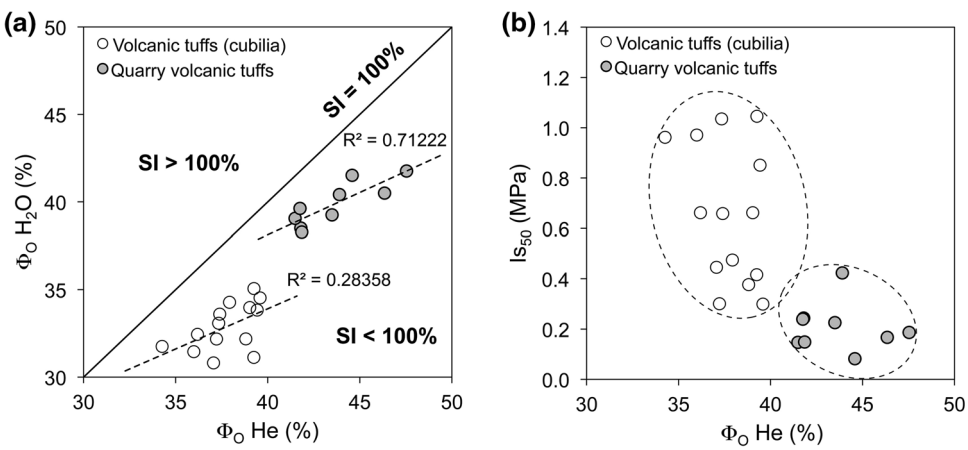

Fig. 11 Physical properties of volcanic tuff: **a** helium open porosity (Φ_OHe) versus water open porosity ($\Phi_O H_2O$) of volcanic stone of *cubilia* and volcanic outcrops; **b** helium open porosity (Φ_OHe) versus point load strength index (Is_{50}) of *cubilia* and volcanic rock from outcrops

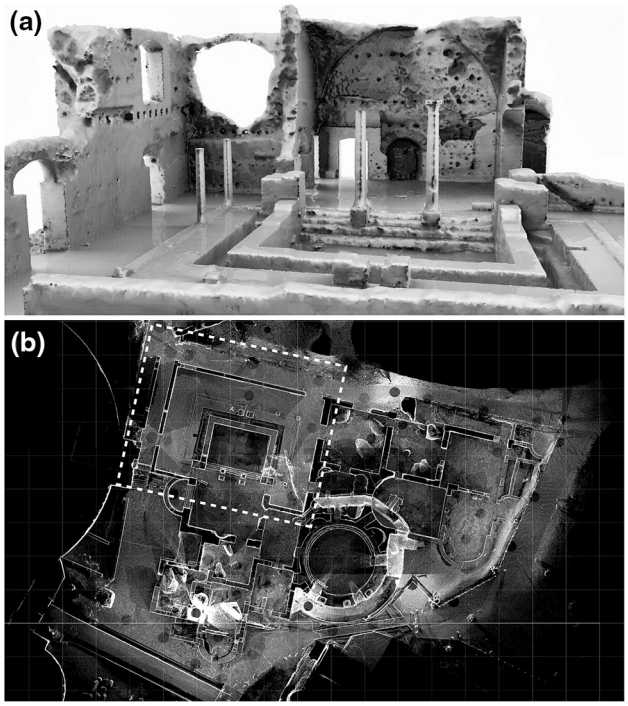

Fig. 12 Laser scan survey: **a** surface model of the *frigidarium* and *natatio* rooms generated from the point cloud (M. Pucci); **b** horizontal section of the general point cloud of *Heliocaminus* Baths where highlights with *dashed line* show *frigidarium* and *natatio*

low thicknesses compared to other mortars, show the higher binder/aggregate ratios (on average 0.87, 0.70, 0.72, respectively; Tables ESM 4 and 5, Online Resources 4 and 5). The first two kinds of mortars were characterized by low values of real density (2.49 and 2.36 g/cm^3, respectively), low values of helium open porosity (38 and 43 %, respectively) and high mechanical strengths (on average 9.47 ± 0.70 and 5.34 ± 3.41 MPa; Table ESM 5, Online Resource 5), probably due to a good mixing before their laying and to the presence of a medium-coarse aggregate (Table ESM 3, Online Resource 3; Fig. 6a). Instead, the coating mortars, considering their different function, have an aggregate less coarse such as not to create problems during the laying of marble slabs on the walls. So, these latter mortars have low bulk density and the highest helium porosity (with average $\rho_B = 1.39$ g/cm^3 and 47.88 %; Table ESM 5, Online Resource 5), resulting in low mechanical strength (0.25 MPa).

By contrast, the floor conglomerates and the vault concretes, considering their structural functions, show lower average values of binder/aggregate ratio (0.59, 0.54, respectively; Tables ESM 4, ESM 5, Online Resources 4 and 5), and, having a less binder percentage with a lowest real density (on average 1.59, 1.50 g/cm^3), show higher real density (2.59, 2.62 g/cm^3) and helium open porosity (42, 47 %). The high porosity of vault concretes, with low bulk density of mortar samples (1.40 g/cm^3) and their binders (0.57 g/cm^3; Tables ESM 5 and 6, Online Resources 5 and 6), is probably due to an insufficient mixing (or compaction) of the casting consequent to the high thickness of the vaults, resulting in low values of mechanical strength (3.76 ± 0.75 MPa; Table ESM 5, Online Resource 5). Considering that the samples of concretes taken from *Heliocaminus* Baths do not include the centimetric and decimetric coarse aggregate (i.e. *caementia* stones) used in the vault castings, it is possible that at the metric scale the porosity of concretes is greater.

Considering their primary constructional function, the floor conglomerates show good mechanical strength ($Is_{(50)}$ 7.45 ± 3.65 MPa; Table ESM 5, Online Resource 5); this is probably due to a better compaction during the casting and to use of a *cocciopesto* aggregate with higher quality and less porosity, as highlighted by higher values of real density ($\rho_R = 2.59 \pm 0.08$ g/cm^3) compared to the wall conglomerates ($\rho_R = 2.36 \pm 0.23$ g/cm^3) where the *cocciopesto* is abundantly used, but with evident difference in its characteristics.

The bedding mortars of bricks and *cubilia* ashlars show intermediate values of binder/aggregate ratio (0.68, 0.62, respectively; Tables ESM 4 and 5, Online Resources 4 and 5), but different characteristics. Inside the group of *cubilia* mortars, the samples ADTH 23 and ADTH 46 have low values of hold mass % in the classes <500 μm (Fig. 6a; Table ESM 3, Online Resource 3) and low strengths (0.37 and 0.32 MPa, respectively; Table ESM 5, Online Resource 5), while the sample ADTH 54, which has a major aggregate sorting (Fig. 6b), shows a greater strength (0.77 MPa; Table ESM 5, Online Resource 5). In the same way, in the brick mortar group, the samples ADTH 4 and ADTH 42, with a major sorting compared to other samples (Fig. 6b), show higher values (0.35 and 0.55 MPa, respectively) compared to the average value of the group (0.26 ± 0.15 MPa).

The physical data of binders calculated indirectly by image analysis and petrographic data show a great variability with very high values of total porosity (average 51–63 %, Table ESM 6, Online Resource 6) and very low values of bulk density (average 0.57–1.24 g/cm^3) compared to those of the aggregates (Table ESM 7, Online Resource 7). However, analysing the mean values and the standard deviations of the mortar groups with different functions in the baths masonry, there are some differences probably related to a different preparation or mixing of mortars made by workers. The wall mortars (i.e. plasters, wall conglomerates and wall-coating mortars), characterized by low thickness, probably were better mixed than the mortars with greater volumes and thicknesses (i.e. concretes, floor-coating mortars), as evidenced by the lower values of closed porosity and related lower standard deviations (Table ESM 5, Online Resource 5).

So, the physical–mechanical tests of this specific case have shown that the resistance of mortars depends on: (1) the porosity, as evidenced by data of the samples ADTH 13, 14 (belonging to the plasters) that have shown lower porosity and higher resistance (around 0.68 MPa) against 0.25–0.53 MPa of other mortars; (2) the sorting degree and particle size of the aggregate, as demonstrated by analysis of samples ADTH 4, 42, 54 belonging to bedding mortars of brick and *cubilia* that are characterized by higher sorting (with modal class between 2000 and 1000 microns) than other mortars, which instead have a modal class on class 4000 microns; (3) characteristics of binder (i.e. bulk density). Subordinately, the strength is influenced by aggregate size compare to those of the specimen and by the thickness of the mortars, as highlighted by high strengths for *arriccio* plasters and low values for vault concretes.

As shown by the edges of the reaction between aggregate and binder, in the case of volcanic aggregate, the hydraulic characteristics are due to volcanic scoria (Fig. 5d, e) that occurs in all the mortars, while the leucitites are chemically inert as well as crystal clasts.

Pozzolanic characteristics are also conferred by *cocciopesto* aggregate, although this latter is present only in some type of mortars, i.e. *trullisatio* (*rinzaffo* layer) of wall conglomerates and *rudus* of floor conglomerates. The reactivity with the binder varies as a function of some physical properties (solid density, porosity, etc.) and colour (that reflects different compositions). The *cocciopesto* aggregate with light colours from yellow to pinkish, characterized by high real density and porosity, seems to have a lower reactivity with binder with respect to *cocciopesto* with more intense colours towards the orange and reddish-orange, probably due to the presence in these latter of a more glassy matrix generated by higher firing temperature. In fact, on observing the physical data (Tables ESM 7 and 8, Online Resources 7 and 8) on the *lateritious* and aggregate samples, it can be seen that: (a) the samples ADTH 2 (*lateritious* 1) with yellow colour have averages of real density and helium open porosity of 2.86 g/cm^3 and 43.25 %, respectively; (b) the samples ADTH 41 (*lateritious* 1) with orange colour have average values of 2.78 g/cm^3 and 35.76 %; (c) the sample ADGT 2 (*lateritious* 2 from "Grandi Terme" baths) with orange-reddish colour has average values of 2.77 g/cm^3 and 43.40 %; (d) the samples ADTH 3c, ADTH 11c, ADTH 18c and ADTH 25c of *cocciopesto* aggregates (from *Heliocaminus* Baths) with orange-reddish colours have averages of real densities and helium open porosity of 2.51 g/cm^3 and 30.68 %. Then, the *lateritious* samples with orange-reddish colour (ADTH 41 and ADGT 2) show greater mechanical resistance (8.19, 2.33 MPa) with respect to the sample with yellowish colour (ADTH 2, 2.08 MPa). Considering that (a) the porosity depends on the shaping of *lateritious* bricks before the firing (pressing, moulding, etc.) and characteristics of raw materials and mixtures (mineralogical composition, size distribution of inclusions) as well as the firing temperature and (b) the solid density and colour depend on the composition (mainly the presence of ferric oxide; Fischer 1983) and firing conditions (temperature, oxidizing or reducing environment of the furnace; Voskuil and van der Giesen 1959; Fischer 1983; Schmidt-Reinholz 1985; Kreimeyer 1987; Stepkowska and Jefferis 1992), the variability of solid density and porosity detected in the analysed *cocciopesto* indicates that this aggregate comes from crushing of various *lateritious* types (bricks, tiles, pottery, earthenware, etc.) made in different productions or with different cooking modes (e.g. temperature).

4.2 Digital survey applications

The final step was to go back to the digital survey and try to bring back all the geological/materials information taken from the samples in the three-dimensional space of the point cloud. This was done using once again the Leica Geosystem Cyclone software and exploiting its tagging function to add notes to the elements in the so-called *model space* (a 3D modelling space coming from a set of one or more point cloud, with full editable features). Each tag was added to a single point in the point cloud, so it was quite easy to locate the sample according to the original notes taken during the on-ground operations, the creation of vertex in different colours and the possibility to turn on and off the point cloud viewing without hiding the tags, which helps in browsing and finding all the tags. The overall result is a "tagged cloud" (Fig. 13) where the set of information taken from the samples is added in their extended form to single points all over the representation of the baths. Each record represented by a tag has its data organized in a table associated with the tag. In this way, it became possible to associate the information from the samples to section slicing, three-dimensional views and any kind of drawing taken from the original dataset. Overall, the enhanced point cloud is itself a better document of the knowledge of the *Heliocaminus* Baths, giving useful information to the archaeologist and being capable of suggesting and to confirming the hypothesis and theories about the development of this complex building.

The point cloud edited with the positioning of all the tags coming from the petrographic and petrophysical characterization of mortars and stones was a useful tool in supporting the study of the *Heliocaminus* Baths. Placing all the data over the point cloud, it was possible to navigate the model and have a rapid, immediate reading of all the available data from this integrated survey. The further interpretation of the samples integrates the remaining

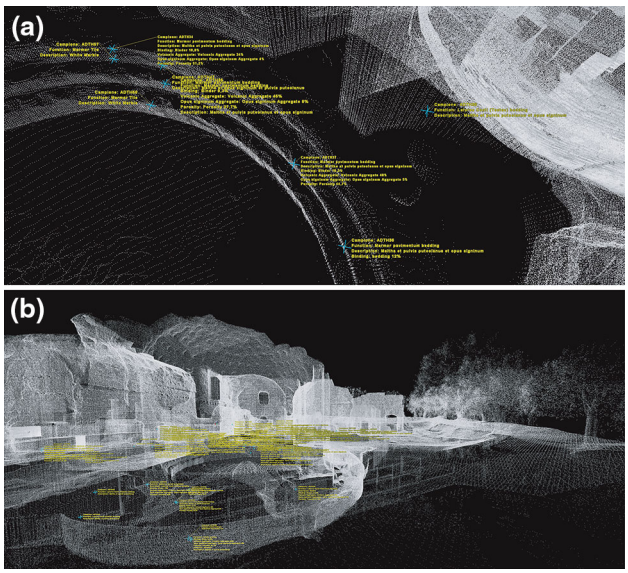

Fig. 13 Laser scan survey: **a** working space in the point cloud model with the tags about the stone samplings; **b** working space in the point cloud model with the tags about the stone samplings

elements with useful metadata; the characteristics of the masonry and of the binders were in their place supporting the interoperation of this complex and ancient architectural masterpiece.

5 Conclusions

The petrophysical characterization together with the architectural–structural analysis and 3D laser scanner survey of the *Heliocaminus* Baths represent a multidisciplinary contribution to the knowledge of: (1) composition and physical properties of mortars and stones, (2) criteria that led Emperor Hadrian and the manufacturers to the choice and supply of materials, (3) dimensions of structure and space distribution of bathrooms.

The results of this research indicate that the construction of the baths respect the general architectural and structural issues of the Roman period. The masonry was constructed using mainly bricks and volcanic stones (used for *cubilia* ashlars) supplied from outcrops located in the area of the Hadrian's Villa about a few hundreds of metres away.

Mortars have been produced using a volcanic aggregate (mainly red and black leucitic basaltic scoria and subordinately leucitites) belonging to the alkaline rocks of ultrapotassic series of the Roman Magmatic Province, outcropping in several points around the area of the Hadrian's Villa. The microscopic analysis highlighted that only basaltic scoria aggregate reacted with binder, while the leucitites, being holocrystalline, did not show reactivity.

Wall conglomerates (*trullisatio* layer) and floor conglomerates (*rudus*) as well as plasters (*arriccio* layers) are produced also using as aggregate the *cocciopesto*, with medium-coarse particle size (until about 18 and 30 mm, respectively). Subordinately, the *cocciopesto* was used also in the floor marble-coating mortars, but in these cases with smaller size (until about 15 and 5 mm, respectively).

The microscopic analysis and physical properties demonstrate that for *cocciopesto*, the Romans used *laterites* with different quality, obtained from crushing of bricks, pottery, tiles, etc. Both *cocciopesto* and the red and black scoria gave pozzolanic characteristics to the mortars, as shown by reaction borders with the binder.

Despite the heterogeneity of the mortar samples analysed, linked also to their small size, the results of physical–mechanical analysis show that the strength is: (1) negatively correlated with the porosity and thickness of mortars; (2) positively correlated with bulk density of binder and with sorting degree of the aggregate.

The use and mode of mixing of aggregate and binder in the production of mortar appear correct according to the standard methods known at the time, even if generally the mortars show a higher binder/aggregate ratio (from 0.5 to 0.9) than that suggested by *Vitruvio* ($0.3 \div 0.5$). Overall, the mortars were prepared correctly with different mixtures in relation to the function in the masonry. However, in some cases, different physical characteristics were detected within groups of samples with the same function in the structure of the baths. Considering that the baths was constructed in a relatively short time (from 118 to 121 AD) with interruptions of yard activities related often to the different construction phases of the villa, it is possible that the mortar production and processing of materials were made quickly and in discontinuous ways, probably with changes of the workforce, as pointed out from the variability of some physical properties (i.e. porosity, density, particle size of aggregate), also among mortars with the same function.

All these variable features, even through the point cloud edited with the positioning of all the tags coming from the petrographic and physical analysis of materials, led us to imagine that there may have been rethinking regarding the design and organization of various spaces or the functionality of the baths (e.g. heating system, where the furnaces beneath the *sudatio* room have never been used for significant periods). The accurate digital survey allowed verifying all the sizes of the walls, making even more readable the differences in the depth of the walls and the changes in masonry works. Considering the results of this research and the historical and archaeological evidences (Verduchi 1975), it can be supposed that the complex represents an "experimental building", where the architects and probably Hadrian himself were testing new

solutions in their personal re-invention of architectonic spaces. In this case, all the traces support the theory of a building of new conception, with advanced technical solutions: so advanced to be tested here for the first time, but with poor results. The following need of reuse of this space brought numerous changes in the technical and building solutions, with minor cure (overall, the personal baths of the emperor were to be erected somewhere else) but with very practical solutions, preserving the main organization and architectonic aspect of the original building.

Acknowledgments Stefano Columbu, Dipartimento di Scienze Chimiche e Geologiche of Cagliari University (UNICA), Italy, was responsible for geomaterial mapping and sampling of the *Heliocaminus* Baths (2010). Giorgio Verdiani, Dipartimento di Architettura of the Florence University (UNIFI), Italy, was responsible for digital survey of the *Heliocaminus* Baths (2010). The operative group of digital survey included: Giorgio Verdiani, Francesco Tioli, Mirco Pucci and Graziano Corsaro, with the collaboration of Alessandro Peruzzi from Area 3D Srl Livorno. All the surveys were carried out during the period of the International Museography Workshop Premio Piranesi: responsible of the workshop: Prof. Pierfederico Caliari. We thank Dr. Benedetta Adembri of the "Soprintendenza per i Beni Archeologici del Lazio" for the support and collaboration.

References

Recommendations Nor.Ma.L. 3/80 (1980) Stone materials: sampling (reprint 1988)

Antonelli F, Columbu S, Lezzerini M, Miriello D (2013) Petrographic characterization and provenance determination of the white marbles used in the Roman sculptures of Forum Sempronii (Fossombrone, Marche, Italy). Appl Phys A 115:1033–1040

Antonelli F, Columbu S, De Vos Raaijmakers M, Andreoli M (2014) An archaeometric contribution to the study of ancient millstones from the Mulargia area (Sardinia, Italy) through new analytical data on volcanic raw material and archaeological items from Hellenistic and Roman North Africa. J Archaeol Sci 50:243–261

Attanasio D, Mesolella G, Pensabene P, Platania R, Rocchi P (2009) EPR and petrographic provenance of the architectural white marbles of three buildings at Villa Adriana. In: Maniatis Y (ed), Asmosia VII. Proceeding 7th international conference ASMOSIA, Thassos 2003, Bull de Corresp Hell Sup, 51, Athens, pp 57–369

Attanasio D, Bruno M, Prochaska W, Yavuz AB (2013) The Asiatic marbles of the Hadrian's Villa at Tivoli. J Archaeol Sci 40:4358–4368

Bernardi A, De Rita D, Funiciello R, Villa IM (1982) Chronology and structural evolution of Alban hills volcanic complex, Latium, Italy. Guidebook AVCEI. Workshop on the explosive volcanism. S. Martino al Cimino, Viterbo

Bertorino G, Franceschelli M, Marchi M, Luglié C, Columbu S (2002) Petrographic characterisation of polished stone axes from Neolithic Sardinia, archaeological implications. Per Miner 71:87–100

Binda L, Baronio G (1986) Indagine sull'aderenza tra legante e laterizio in malte ed intonachi di *cocciopesto*. Boll d'Arte 35(36):109–115

Camiz A (2004) La cosiddetta "Roccabruna" ed il dies imperii. In: Basso Peressut L, Caliari PF (eds) Villa Adriana. Environments. Milano, vol. 2, pp 121–129

Cicerchia P (1985) Sul carattere distributivo delle terme con Heliocaminus di Villa Adriana. Xenia 9:47–60

Collepardi M (1993) La produzione del calcestruzzo antico e moderno. Atti del Convegno di Studi «Calcestruzzi antichi e moderni: Storia, Cultura e Tecnologia». Bressanone, Libreria Progetto Editore, Padova, pp 181–192

Columbu S, Verdiani G (2011) From the small elements to the urban scale: An investigation where petrophysical study of materials and architectural shape analysis try to read a masterplan in the Hadrian's Villa, Tivoli (Rome, Italy). In: Proceedings of 16th international conference on cultural heritage and new technologies (CHNT 2011) Wien. 14–16 November 2011, Urban archaeology and prospection, Museen der Stadt Wien—Stadtarchäologie. vol 1, part 3, pp 273–293

Columbu S, Verdiani G (2014) Digital survey and material analysis strategies for documenting, monitoring and study the romanesque churches in Sardinia, Italy, lecture notes in computer science, vol 8740. Springer, Heidelberg, pp 446–453

Columbu S, Guccini G, Verdiani G (2013) Petro-physical characterization and 3D digital modeling for geometric reconstruction of the Neolithic "domus de janas" of Sedini field (North-Sardinia, Italy). Adv Comput Sci Int J 2(5):70–80

Columbu S, Antonelli F, Lezzerini M, Miriello D, Adembri B, Blanco A (2014a) Provenance of marbles used in the *Heliocaminus* Baths of Hadrian's Villa (Tivoli, Italy). J Archaeol Sci 49:332–342

Columbu S, Gioncada A, Lezzerini M, Marchi M (2014b) Hydric dilatation of ignimbritic stones used in the church of Santa Maria di Otti (Oschiri, northern Sardinia, Italy). Ital J Geosci 133:149–160

Columbu S, Cruciani G, Fancello D, Franceschelli M, Musumeci G (2015) Petrophysical properties of a granite–protomylonite–ultramylonite sequence: insight from the Monte Grighini shear zone, central Sardinia, Italy. Eur J Miner 27:471–486

Crisci GM, De Francesco AM, Gagliardi F, Mercurio P, Gattuso P, Miriello D (2002) L'analisi composizionale delle malte: Un valido mezzo per risalire alle fasi costruttive. Risultati preliminari. In: D'Amico C (ed) Proceedings of II Congresso nazionale di archeometria. Pàtron editore, Bologna, pp 485–494

De Luca R, Cau Ontiveros MA, Miriello D, Pecci A, Le Pera E, Bloise A, Crisci GM (2013) Archaeometric study of mortars and plasters from the Roman City of Pollentia (Mallorca-Balearic Islands). Per Miner 82:353–379

Fischer P (1983) Anmerkungen zur Brennfarbe von Tonen. Ceramic Forum International. Berichte Deutsche Heramische Gesellschaft 8:320–327

ISRM International Society For Rock Mechanics (1972) Suggest method for determining the point load strength index. ISRM (Lisbon, Portugal). Committee on field tests. Document n.1, pp. 8–12

ISRM, International Society For Rock Mechanics (1985) Suggest method for determining the point load strength. ISRM commission for testing methods, Working group on revision of the point load test methods. Int J Rock Mech Min Sci Geomech Abstr 22:51–60

Kreimeyer R (1987) Some notes on the firing colour of clays bricks. Appl Clay Sci 2:175–183

Lapuente P, León P, Nogales T, Royo H, Preite-Martinez M, Blanc Ph (2012) White sculptural materials from Villa Adriana: study of provenance. In: Gutiérrez Garcia A, Lapuente P, Rodà I (eds) Interdisciplinary studies on ancient stone. Proceedings of the IX ASMOSIA conference, Tarragona, pp 364–375

Lezzerini M, Antonelli F, Columbu S, Gadducci R, Marradi A, Miriello D, Parodi L, Secchiari L, Lazzeri A (2014) The documentation and conservation of the cultural heritage: 3D laser scanning and GIS techniques for thematic mapping of the stonework of the façade of St. Nicholas church (Pisa, Italy). Int J Archit Herit Conserv Anal Restor. doi:10.1080/15583058.2014.924605

MacDonald WL, Pinto JA (2006) Villa Adriana; la costruzione e il mito da Adriano a Louis I Kahn. Architettura Paperback, Mondadori Electa, Milano, p 400

Macciotta G, Bertorino G, Caredda A, Columbu S, Coroneo R, Franceschelli M, Marchi M, Rescic S (2001) The S.Antioco of Bisarcio Basilica (NE Sardinia, Italy): water-rock interaction in ignimbrite monument decay. In: Cidu, Swets, Zeitlinger, Lisse (eds) Water–rock interaction (WRI-10). Balkema, Rotterdam, pp 415–418

Maravelaki-Kalaitzaki P, Bakolas A, Moropoulou A (2003) Physico-chemical study of Cretan ancient mortars. Cem Concr 33:651–661

Melis S, Columbu S (2000) Matériaux de construction en époque romaine et aves les anciennes carrières: l'exemple du théâtre de Nora (Sardaigne SO, Italie). In: Lorenz J, Tardy D, Coulon G (eds) Proceedings of La pierre dans la ville antique et médiévale. Analyse méthodologie et apports, Argenton sur Creuse, France, 29–31 March 1998. Saint-Marcel, Musée d'Argentomagus (ed), pp 103–117

Miriello D, Barca D, Bloise A, Ciarallo A, Crisci GM, De Rose T, Gattuso C, Gazineo F, La Russa F (2010) Characterisation of archaeological mortars from Pompeii (Campania, Italy) and identification of construction phases by compositional data analysis. J Archaeol Sci 37:2207–2223

Miriello D, Antonelli F, Apollaro C, Bloise A, Bruno N, Catalano E, Columbu S, Crisci GM, De Luca R, Lezzerini M, Mancuso S, La Marca A (2015) New data about the ancient mortars from the archaeological site of Kyme (Turkey): compositional characterization. Per Miner **(in print)**

Morbidelli L (2003) In: Le rocce e i loro costituenti. Bardi Editore, Roma

Palmström A (1995) RMi—a rock mass characterization system for rock engineering purposes. Ph D. thesis, University of Oslo, Norway, 430 pp

Peccerillo A (2005) Plio-quaternary volcanism in italy. petrology, geochemistry, geodynamics. Springer, Heidelberg, p 365

Pensabene P, Antonelli F, Lazzarini L, Cancelliere S (2012) Provenance of marble sculptures and artifacts from the so-called Canopus and other buildings of "Villa Adriana" (Hadrian's Villa, Tivoli, Italy). J Archaeol Sci 39:1331–1337

Pollione MV (15 BC) De Architecture. Vol. II. In: Cesariano C, De Architectura Libri Dece, 1521, Como

Salvatori A, Trucchi D, Guidobaldi F (1988) The marbles used in the decorations of Hadrian's Villa at Tivoli. In: Herz N, Walelkens M (eds) Classical marble: geochemistry, technology, trade. Kluwer Academic Publishers, Dordrecht, pp 177–185

Salza Prina Ricotti E (2000) Villa Adriana, il sogno di un imperatore. L'Erma di Bretschneider, Rome

Schmidt-Reinholz Ch (1985) Remarks on the complete colouration of heavy-clay bodies. Interbrick 1(3):36–38

Stepkowska ET, Jefferis SA (1992) Influence of microstructure on firing colour of clays. Appl Clay Sci 6:319–342

Verdiani G, Columbu S (2010) E. Stone, an archive for the Sardinia monumental witnesses. Third International Conference, Euro-Med 2010, Lemessos, Cyprus, November 8–13, 2010. Lecture Notes in Computer Science (LNCS), Springer, Heidelberg, vol 6436/2010, pp 356–372

Verduchi P (1975) Le Terme con cosiddetto Heliocaminus a Villa Adriana. Quaderni dell'Istituto di Topografia Antica, Università di Roma 8:55–95

Vola G, Gotti E, Brandon C, Oleson JP, Hohlfelder RL (2011) Chemical, mineralogical and petrographic characterization of roman ancient hydraulic concretes cores from Santa Liberata, Italy, and Caesarea Palestinae, Israel. Per Miner 80:317–338

Voskuil J, Van Der Giesen D (1959) Die Farbbildung in roten und gelben Ziegelsteinen. Sprechsaal 92:529–533

ESM Tables

Title: **Contribution of petrophysical analysis and 3D digital survey in the archaeometric investigations of the Emperor Hadrian's Baths (Tivoli, Italy) -** Journal: **Rendiconti Lincei**

Author: **Stefano Columbu*, Fabio Sitzia, Giorgio Verdiani**

*Corresponding author: *columbus@unica.it*, *Dipartimento di Scienze Chimiche e Geologiche, University of Cagliari, Italy*

Sample typology	Sample	Room of provenance	Height from internal floor (cm)
Brick bedding mortars	ADTH 4	*Calidarium*	-98
	ADTH 6	*Calidarium*	-35
	ADTH 11	*Boilers room*	-85
	ADTH 21	*Natatio*	90
	ADTH 35	*Sudatio*	-16
	ADTH 42	*Sudatio*	-98
	ADTH 43	*Sudatio*	7
Cubilia bedding mortars	ADTH 23	*Natatio*	58
	ADTH 46	*Sudatio*	-23
	ADTH 54	*Apodyterium*	107
Floor-coating bedding mortars	ADTH 24	*Natatio*	-25
	ADTH 28	*Natatio*	-138
	ADTH 34	*Sudatio*	-4
	ADTH 37	*Laconicum*	-64
Wall-coating bedding mortars	ADTH 7	*Calidarium*	28
	ADTH 31	*Laconicum*	25
	ADTH 52	*Apodyterium*	20
Floor conglomerates *(rudus)*	ADTH 3	*Calidarium*	-10
	ADTH 15	*Tepidarium*	-12
	ADTH 25	*Natatio*	-28
	ADTH 32	*Laconicum*	-7
	ADTH 33	*Laconicum*	-5
Wall conglomerates *(trullisatio)*	ADTH 18	*Frigidarium*	30
	ADTH 26	*Natatio*	-109
	ADTH 58	*Apodyterium*	26
Vault concretes	ADTH 12	*Calidarium*	0
	ADTH 50	*Apodyterium*	52
	ADTH 53	*Apodyterium*	58
Plasters (*arriccio*)	ADTH 13	*Tepidarium*	-7
	ADTH 14	*Calidarium*	40
Volcanic scoria aggregates	ADTH 33 b	*Laconicum*	/
	ADTH 18 b	*Frigidarium*	/
	ADTH 50 b	*Apodyterium*	/
	ADTH 11 b	*Boilers room*	/
	ADTH 34 b	*Sudatio*	/
	ADTH 14 b	*Calidarium*	/
	ADTH 12 b	*Calidarium*	/
Leucitite aggregates	ADTH 35 l	*Sudatio*	/
	ADTH 58 l	*Apodyterium*	/
	ADTH 25 l	*Natatio*	/
Cocciopesto aggregates	ADTH 18 c	*Frigidarium*	/
	ADTH 25 c	*Natatio*	/
	ADTH 3 c	*Calidarium*	/
	ADTH 11 c	*Boilers room*	/
Lateritious 1	ADTH 2	*Calidarium*	-30
	ADTH 41	*Sudatio*	-95
Lateritious 2	ADGT 2	*Grandi terme*	30
Cubilia volcanic tuff	ADTH 54	*Apodyterium*	107
	ADTH 8	*Calidarium*	0
	ADTH 23	*Natatio*	58
Quarry volcanic tuff	ADCA 1	*Quarry outcrops*	/
	ADCA 2		/

Tab. ESM1 Sampled materials from the building of the *Heliocaminus* Baths (see the map of *Heliocaminus* Baths with sampling points of Fig. 5)

Mortar typology	Sample	Basalt scoria	Leucitite	*Cocciopesto*	Marble	Clinopyroxene	Green Hornblende	Biotite	Total aggregate
Brick bedding mortars	ADTH 4	99.5	0	0	0.5	0	0	0	100
	ADTH 6	99.1	0.7	0	0.2	0	0	0	100
	ADTH 11	98.2	1.5	0	0	0.3	0	0	100
	ADTH 21	99.8	0	0	0.2	0	0	0	100
	ADTH 35	94.3	3.8	0	0	1.9	0	0	100
	ADTH 42	96.8	1.1	0	0.1	0.9	1.1	0	100
	ADTH 43	99.4	0	0	0.6	0	0	0	100
Cubilia bedding mortars	ADTH 23	99.9	0	0	0.1	0	0	0	100
	ADTH 46	97.8	0.8	0	0.2	1.2	0	0	100
	ADTH 54	95.7	2.1	0	0.3	1.2	0.7	0	100
Floor-coating bedding mortars	ADTH 24	95.4	0	4.3	0	0	0.3	0	100
	ADTH 28	87.9	1	5.1	0	1	4	1	100
	ADTH 34	95.2	0	4.8	0	0	0	0	100
	ADTH 37	95.1	0	4.5	0	0.4	0	0	100
Wall-coating bedding mortars	ADTH 7	98	0	0	0	1	1	0	100
	ADTH 31	98.3	0.8	0	0	0	0.9	0	100
	ADTH 52	99.3	0	0	0	0.7	0	0	100
Floor conglomerates *(rudus)*	ADTH 3	85.7	0	13.8	0	0.5	0	0	100
	ADTH 15	87.9	0	12.1	0	0	0	0	100
	ADTH 25	79.8	3.2	15.2	0	1.8	0	0	100
	ADTH 32	78.7	5.1	16.2	0	0	0	0	100
	ADTH 33	81	2.1	15.3	0	0	1.6	0	100
Wall conglomerates *(trullisatio)*	ADTH 18	73.1	7.7	17.7	0	0.9	0.6	0	100
	ADTH 26	76.5	2.7	20.4	0	0	0.4	0	100
	ADTH 58	85.1	1.1	13.8	0	0	0	0	100
Vault concretes	ADTH 12	98.5	0.9	0	0.1	0	0.5	0	100
	ADTH 50	98.7	0	0	0.1	1.2	0	0	100
	ADTH 53	99.8	0	0	0.2	0	0	0	100
Plasters (*arriccio*)	ADTH 13	84.4	5.2	8.2	0	0	2.2	0	100
	ADTH 14	81.7	0	16.6	0	1.4	0.3	0	100

Tab. ESM2 Modal analysis with percentage of different aggregates present in the mortars

Mortars typology	Sample	Particle diameter (μm)						
		4000	2000	1000	500	250	125	63
Brick bedding mortars	ADTH 4	18.99	18.06	22.14	20.64	9.26	6.72	4.18
	ADTH 6	49.07	13.36	10.71	9.42	8.02	6.74	2.69
	ADTH 11	58.03	15.80	11.09	7.00	3.57	2.97	1.54
	ADTH 21	35.10	29.47	12.51	9.81	5.95	4.42	2.73
	ADTH 35	60.80	13.45	10.73	6.58	5.97	1.65	0.82
	ADTH 42	18.85	36.91	19.51	8.99	8.02	4.95	2.76
	ADTH 43	41.54	18.32	13.37	9.26	8.78	6.46	2.27
	Mean	40.34	20.77	14.29	10.24	7.08	4.84	2.43
	S.D.	17.10	8.97	4.63	4.75	2.01	1.98	1.06
Cubilia bedding mortars	ADTH 23	55.01	22.00	14.29	3.11	2.36	1.80	1.44
	ADTH 46	75.99	9.94	4.13	3.83	3.43	1.64	1.04
	ADTH 54	26.12	20.71	20.34	18.57	7.58	4.09	2.59
	Mean	52.37	17.55	12.92	8.51	4.45	2.51	1.69
	S.D.	25.04	6.62	8.19	8.73	2.76	1.37	0.80
Floor-coating bedding mortars	ADTH 24	33.63	16.71	13.62	13.45	9.95	8.48	4.16
	ADTH 28	11.47	20.79	16.86	15.68	16.05	15.07	4.09
	ADTH 34	30.07	27.03	16.04	11.17	9.45	4.36	1.87
	ADTH 37	5.91	35.00	23.37	16.13	9.65	6.18	3.77
	Mean	20.27	24.88	17.47	14.11	11.27	8.52	3.47
	S.D.	13.64	7.97	4.17	2.28	3.19	4.68	1.08
Wall-coating bedding mortars	ADTH 7	60.13	11.75	10.15	7.57	5.43	3.43	1.54
	ADTH 31	28.00	23.90	21.33	11.45	7.85	4.52	2.95
	ADTH 52	31.63	30.18	16.27	9.78	5.72	3.95	2.46
	Mean	39.92	21.94	15.92	9.60	6.33	3.97	2.32
	S.D.	17.60	9.37	5.60	1.95	1.32	0.54	0.71
Floor conglomerates *(rudus)*	ADTH 3	63.27	11.40	4.43	4.10	2.87	2.00	0.91
	ADTH 15	62.55	14.31	11.55	5.92	2.54	2.00	1.13
	ADTH 25	70.53	13.58	6.53	3.74	2.61	1.74	1.27
	ADTH 32	57.45	13.01	10.32	7.99	4.22	3.93	3.09
	ADTH 33	65.44	12.21	6.54	5.20	4.90	3.32	2.38
	Mean	63.85	12.90	7.87	5.39	3.43	2.60	1.76
	S.D.	4.75	1.14	2.96	1.69	1.07	0.97	0.94
Wall conglomerates *(trullisatio)*	ADTH 18	38.26	19.69	13.79	8.31	8.91	6.84	4.21
	ADTH 26	34.17	23.57	15.60	11.14	7.92	4.79	2.81
	ADTH 58	59.24	14.59	9.57	6.82	5.09	3.04	1.64
	Mean	43.89	19.28	12.99	8.76	7.31	4.89	2.89
	S.D.	13.45	4.50	3.09	2.20	1.98	1.90	1.28
Vault concretes	ADTH 12	23.09	33.91	16.00	10.78	7.88	5.12	3.22
	ADTH 50	22.88	30.32	16.83	10.20	9.42	7.31	3.06
	ADTH 53	32.17	23.51	14.50	12.21	8.31	6.02	3.27
	Mean	26.05	29.25	15.78	11.06	8.54	6.15	3.18
	S.D.	5.31	5.28	1.18	1.04	0.79	1.10	0.11
Plasters (*arriccio*)	ADTH 13	58.63	22.23	9.17	4.51	3.35	1.31	0.81
	ADTH 14	68.16	10.94	6.17	5.23	4.81	3.16	1.54
	Mean	63.39	16.58	7.67	4.87	4.08	2.23	1.18
	S.D.	6.74	7.98	2.12	0.51	1.03	1.31	0.52

Tab. ESM3 Results of particle-size analysis of mortar aggregates with size-distribution in the classes 4000, 2000, 1000, 500, 250, 125, 63 μm
Abbreviations: S.D. = standard deviation

Mortars typology	Sample	Cubic specimen data									Thin section samples data		
		Face 1 A (%)	Face 2 A (%)	Face 3 A (%)	Face 4 A (%)	Face 5 A (%)	Face 6 A (%)	Mean A (%)	Mean B (%)	B/A	Mean A (%)	Mean B (%)	B/A
Brick bedding mortars	ADTH 4	56.00	51.27	71.78	71.04	71.77	58.03	63.31	36.69	0.58	63.15	36.85	0.58
	ADTH 6	69.81	64.59	72.86	43.88	66.76	74.32	65.37	34.63	0.53	55.04	44.96	0.82
	ADTH 11	42.26	49.87	47.72	55.81	51.21	64.81	51.95	48.05	0.93	63.9	36.10	0.56
	ADTH 21	62.96	41.77	67.92	52.46	61.74	67.63	59.08	40.92	0.69	60.68	39.32	0.65
	ADTH 35	77.64	77.00	66.93	66.69	74.11	70.18	72.09	27.91	0.39	61.95	38.05	0.61
	ADTH 42	47.27	51.17	54.13	47.22	55.82	50.06	50.95	49.06	0.96	40.19	59.81	1.49
	ADTH 43	62.70	66.51	49.74	67.01	65.04	49.85	60.14	39.86	0.66	52.05	47.95	0.92
Cubilia bedding mortars	ADTH 23	71.05	58.52	61.87	62.41	55.85	54.68	60.73	39.27	0.65	48.69	51.31	1.05
	ADTH 46	47.57	53.28	64.31	55.04	68.93	57.49	57.77	42.23	0.73	48.35	51.65	1.07
	ADTH 54	77.11	67.61	54.15	62.01	64.23	77.11	67.04	32.96	0.49	48.87	51.13	1.05
Floor-coating bedding mortars	ADTH 24	70.26	55.63	67.23	59.42	65.55	62.01	63.35	36.65	0.58	46.6	53.40	1.15
	ADTH 28	71.79	70.63	65.25	69.97	70.01	68.43	69.35	30.65	0.44	44.55	55.45	1.24
	ADTH 34	50.54	79.88	52.71	69.93	64.20	72.98	65.04	34.96	0.54	35.61	64.39	1.81
	ADTH 37	45.41	44.08	46.62	55.66	54.54	57.44	50.63	49.38	0.98	37.1	62.90	1.70
Wall-coating bedding mortars	ADTH 7	69.81	64.58	43.88	72.85	39.87	66.00	59.50	40.50	0.68	38.66	61.34	1.59
	ADTH 31	54.85	54.87	57.73	54.92	59.11	46.16	54.61	45.39	0.83	40.12	59.88	1.49
	ADTH 52	66.97	67.21	50.78	57.17	60.11	62.55	60.80	39.20	0.64	40.04	59.96	1.50
Floor conglomerates *(rudus)*	ADTH 3	58.03	63.41	56.84	75.26	69.42	74.81	66.29	33.71	0.51	62.27	37.73	0.61
	ADTH 15	55.33	55.28	48.91	69.44	59.02	63.71	58.62	41.39	0.71	59.81	40.19	0.67
	ADTH 25	57.28	71.11	72.63	73.27	65.18	54.11	65.60	34.40	0.52	45.46	54.54	1.20
	ADTH 32	62.49	52.40	66.78	65.11	69.33	58.32	62.41	37.60	0.60	50.5	49.50	0.98
	ADTH 33	64.14	65.72	69.13	60.21	55.19	59.23	62.27	37.73	0.61	48.55	51.45	1.06
Wall conglomerates *(trullisatio)*	ADTH 18	57.94	60.75	57.58	54.31	60.54	67.27	59.73	40.27	0.67	49.03	50.97	1.04
	ADTH 26	43.47	57.58	42.95	61.97	57.21	60.04	53.87	46.13	0.86	52.19	47.81	0.92
	ADTH 58	64.30	59.67	59.04	67.37	67.19	67.44	64.17	35.83	0.56	60.97	39.03	0.64
Vault concretes	ADTH 12	55.43	71.94	60.89	54.45	72.31	61.78	62.80	37.20	0.59	36.02	63.98	1.78
	ADTH 50	77.11	71.41	58.81	63.21	70.34	66.34	67.87	32.13	0.47	32.62	67.38	2.07
	ADTH 53	51.98	66.48	53.52	69.10	67.20	75.99	64.05	35.96	0.56	37.44	62.56	1.67
Plasters (*arriccio*)	ADTH 13	49.73	42.91	49.01	47.55	51.68	44.02	47.48	52.52	1.11	53.4	46.60	0.87
	ADTH 14	52.01	63.18	64.14	66.34	66.11	57.19	61.49	38.51	0.63	49.39	50.61	1.02

Tab. ESM4 Comparison of binder/aggregate ratio (B/A) by image analysis on six faces of pseudo-cubic specimens and on thin sections. The aggregate's percentage calculated on the specimens is obtained by the arithmetic mean of the aggregate percentages of six faces.
Abbreviations: A = aggregate; B = binder

Mortar typology	Sample	ρ_R	ρ_B	$\Phi_O He$	$\Phi_O H_2O$	CI_W	SI	Is_{50}	R_C	R_T	B/A
		(g/cm^3)	(g/cm^3)	(%)	(%)	(%)	(%)	(MPa)	(MPa)	(MPa)	
Brick bedding mortars	ADTH 4	2.66	1.36	48.82	42.91	31.32	87.90	0.35	4.84	0.43	0.58
	ADTH 6	2.65	1.42	46.21	38.33	26.80	82.95	0.11	1.51	0.13	0.53
	ADTH 11	2.71	1.49	45.13	41.73	27.94	92.46	0.14	1.90	0.17	0.93
	ADTH 21	2.40	1.35	43.82	40.12	28.49	91.55	0.15	2.14	0.19	0.69
	ADTH 35	2.43	1.51	37.70	37.00	24.36	98.15	0.25	3.45	0.31	0.39
	ADTH 42	2.61	1.57	39.83	35.65	22.61	89.51	0.55	7.69	0.69	0.96
	ADTH 43	2.48	1.49	39.96	37.65	25.19	94.21	0.28	3.85	0.34	0.66
	Mean	2.56	1.46	43.07	39.06	26.67	90.96	0.26	3.62	0.32	0.68
	S.D.	0.12	0.08	4.01	2.63	2.90	4.84	0.15	2.15	0.19	0.21
Cubilia bedding mortars	ADTH 23	2.69	1.36	49.59	41.86	30.63	84.41	0.37	5.17	0.46	0.65
	ADTH 46	2.70	1.51	44.12	36.79	24.20	83.37	0.32	4.55	0.41	0.73
	ADTH 54	2.50	1.47	41.02	39.53	26.56	96.35	0.77	10.71	0.96	0.49
	Mean	2.63	1.45	44.91	39.39	27.13	88.05	0.49	6.81	0.61	0.62
	S.D.	0.11	0.08	4.34	2.54	3.25	7.21	0.24	3.39	0.30	0.12
Floor-coating bedding mortars	ADTH 24	2.52	1.38	45.30	43.80	31.44	96.70	0.18	2.54	0.23	0.58
	ADTH 28	2.75	1.57	43.23	37.19	23.63	86.03	0.11	1.60	0.14	0.44
	ADTH 34	2.60	1.27	51.19	47.01	36.68	91.83	0.37	5.12	0.46	0.54
	ADTH 37	2.51	1.39	44.72	41.17	29.50	92.06	0.45	6.26	0.56	0.98
	Mean	2.60	1.40	46.11	42.29	30.31	91.66	0.28	3.88	0.35	0.63
	S.D.	0.11	0.12	3.50	4.16	5.39	4.37	0.16	2.17	0.19	0.24
Wall-coating bedding mortars	ADTH 7	2.64	1.40	47.17	37.53	26.71	79.56	0.08	1.17	0.10	0.68
	ADTH 31	2.68	1.49	44.48	37.41	25.04	84.12	0.37	5.18	0.46	0.83
	ADTH 52	2.61	1.25	51.98	45.56	35.99	87.64	0.31	4.34	0.39	0.64
	Mean	2.64	1.38	47.88	40.17	29.24	83.77	0.25	3.56	0.32	0.72
	S.D.	0.03	0.12	3.80	4.67	5.90	4.05	0.15	2.12	0.19	0.10
Floor conglomerates *(rudus)*	ADTH 3	2.67	1.56	41.37	40.14	25.48	97.04	0.95	13.32	1.19	0.51
	ADTH 15	2.59	1.49	42.70	36.73	24.63	86.02	0.47	6.64	0.59	0.71
	ADTH 25	2.48	1.40	43.57	39.56	26.96	90.78	0.57	7.98	0.71	0.52
	ADTH 32	2.54	1.47	41.99	36.72	24.80	87.44	0.41	5.73	0.51	0.60
	ADTH 33	2.65	1.57	40.98	36.36	23.11	88.73	0.26	3.57	0.32	0.61
	Mean	2.59	1.50	42.12	37.90	25.00	90.00	0.53	7.45	0.66	0.59
	S.D.	0.08	0.07	1.04	1.80	1.40	4.31	0.26	3.65	0.33	0.08
Wall conglomerates *(trullisatio)*	ADTH 18	2.62	1.35	48.43	39.06	28.66	80.64	0.11	1.48	0.13	0.67
	ADTH 26	2.25	1.21	46.38	44.94	36.96	96.89	0.47	6.56	0.59	0.86
	ADTH 58	2.21	1.46	34.14	32.81	22.31	96.08	0.57	7.97	0.71	0.56
	Mean	2.36	1.34	42.99	38.93	29.31	91.20	0.38	5.34	0.48	0.70
	S.D.	0.23	0.13	7.72	6.07	7.35	9.15	0.24	3.41	0.30	0.15
Vault concretes	ADTH 12	2.56	1.46	42.79	37.80	25.65	88.33	0.25	3.46	0.31	0.59
	ADTH 50	2.66	1.36	49.02	44.55	32.58	90.88	0.23	3.21	0.29	0.47
	ADTH 53	2.63	1.37	47.83	42.07	30.35	87.93	0.33	4.61	0.41	0.56
	Mean	2.62	1.40	46.55	41.47	29.53	89.05	0.27	3.76	0.34	0.54
	S.D.	0.05	0.06	3.30	3.41	3.54	1.60	0.05	0.75	0.07	0.06
Plasters (*arriccio*)	ADTH 13	2.44	1.55	36.64	36.19	23.28	98.79	0.64	8.98	0.80	1.11
	ADTH 14	2.54	1.53	39.64	37.82	24.59	95.40	0.71	9.96	0.89	0.63
	Mean	2.49	1.54	38.14	37.01	23.94	97.09	0.68	9.47	0.85	0.87
	S.D.	0.07	0.01	2.13	1.15	0.92	2.40	0.05	0.70	0.06	0.34

Tab. ESM5 Physical properties of mortars and binder/aggregate ratio (B/A)

Abbreviations: S.D. = standard deviation; ρ_R = real density; ρ_B = bulk density; $\Phi_O He$ = helium open porosity; $\Phi_O H_2O$ = water open porosity; CI_W = water imbibition coefficient; SI = water saturation index; Is_{50} = Point Load strength index; R_C = compression strength; R_T = tensile strength

Binder and aggregate	Sample	ρ_R	ρ_B	$\Phi_O He$	$\Phi_C He$	Φ_T	$\Phi_O H_2O$	CI_W	SI	B/A
		(g/cm^3)	(g/cm^3)	(%)	(%)	(%)	(%)	(%)	(%)	
Brick bedding mortar binders	ADTH 4	1.67	0.58	39.61	13.88	53.49	31.52	26.39	79.57	0.58
	ADTH 6	1.52	0.60	33.17	18.19	51.35	22.37	17.94	67.44	0.53
	ADTH 11	2.67	1.28	49.49	2.16	51.65	44.20	30.86	89.31	0.93
	ADTH 21	1.53	0.71	36.57	21.00	57.58	31.55	25.08	86.25	0.69
	ADTH 35	0.81	0.48	15.77	41.53	57.30	16.08	11.50	101.94	0.39
	ADTH 42	2.57	1.47	41.43	4.74	46.17	34.46	21.81	83.17	0.96
	ADTH 43	1.59	0.90	28.99	24.39	53.38	26.38	18.83	91.00	0.66
	Mean	1.77	0.86	35.00	17.99	52.99	29.51	21.77	85.53	0.68
	S.D.	0.65	0.38	10.68	13.21	3.90	9.03	6.37	10.66	0.21
Cubilia bedding mortar binders	ADTH 23	1.90	0.66	44.02	11.20	55.23	32.53	27.26	73.90	0.65
	ADTH 46	2.13	1.01	39.32	11.35	50.67	27.85	19.13	70.84	0.73
	ADTH 54	1.18	0.58	24.58	28.64	53.23	23.60	17.19	95.99	0.49
	Mean	1.74	0.75	35.97	17.07	53.04	28.00	21.19	80.24	0.62
	S.D.	0.50	0.23	10.14	10.03	2.28	4.47	5.34	13.72	0.12
Floor-coating bedding mortar binders	ADTH 24	1.44	0.59	34.25	19.95	54.20	33.24	26.80	97.07	0.58
	ADTH 28	1.42	0.60	27.40	20.79	48.19	20.01	12.73	73.05	0.44
	ADTH 34	1.47	0.38	41.37	12.17	53.54	36.32	33.53	87.78	0.54
	ADTH 37	2.43	1.16	51.14	6.32	57.46	45.48	35.48	88.95	0.98
	Mean	1.69	0.68	38.54	14.81	53.35	33.77	27.13	86.71	0.63
	S.D.	0.49	0.34	10.15	6.86	3.84	10.54	10.30	10.00	0.24
Wall-coating bedding mortar binders	ADTH 7	1.90	0.74	42.37	12.62	54.98	27.38	22.16	64.61	0.68
	ADTH 31	2.36	1.13	44.19	7.50	51.69	32.50	22.96	73.54	0.83
	ADTH 52	1.76	0.48	48.10	10.12	58.22	38.76	36.16	80.59	0.64
	Mean	2.01	0.78	44.89	10.08	54.97	32.88	27.09	72.91	0.72
	S.D.	0.31	0.33	2.93	2.56	3.26	5.70	7.86	8.01	0.10
Floor conglomerate *(rudus)* binders	ADTH 3	1.49	0.77	25.88	23.93	49.81	25.66	16.26	99.13	0.51
	ADTH 15	1.90	0.95	36.03	16.19	52.22	27.42	19.63	76.11	0.71
	ADTH 25	1.23	0.50	30.86	22.69	53.55	26.43	19.71	85.64	0.52
	ADTH 32	1.53	0.74	31.34	22.20	53.53	24.65	18.24	78.66	0.60
	ADTH 33	1.71	0.89	30.06	20.12	50.18	24.32	15.56	80.90	0.61
	Mean	1.57	0.77	30.83	21.03	51.86	25.69	17.88	84.09	0.59
	S.D.	0.25	0.17	3.62	3.03	1.79	1.27	1.91	9.11	0.08
Wall conglomerate *tTrullisatio)* binders	ADTH 18	1.83	0.60	46.09	11.53	57.62	32.23	27.23	69.92	0.67
	ADTH 26	1.64	0.63	50.31	15.79	66.10	49.47	47.19	98.34	0.86
	ADTH 58	0.92	0.68	16.63	49.72	66.35	16.19	12.62	97.33	0.56
	Mean	1.46	0.64	37.68	25.68	63.36	32.63	29.01	88.53	0.70
	S.D.	0.48	0.04	18.35	20.92	4.97	16.65	17.35	16.12	0.15
Vault concrete binders	ADTH 12	1.54	0.75	30.80	21.87	52.67	24.09	17.90	78.22	0.59
	ADTH 50	1.38	0.41	35.04	14.93	49.97	29.68	25.12	84.69	0.47
	ADTH 53	1.58	0.57	37.08	15.77	52.86	29.32	24.24	79.07	0.56
	Mean	1.50	0.57	34.31	17.52	51.83	27.70	22.42	80.66	0.54
	S.D.	0.10	0.17	3.21	3.79	1.62	3.13	3.94	3.52	0.06
Plasters (*arriccio*) binders	ADTH 13	2.58	1.61	41.49	5.00	46.49	42.08	27.53	101.40	1.11
	ADTH 14	1.58	0.87	28.60	23.90	52.49	27.31	18.28	95.50	0.63
	Mean	2.08	1.24	35.05	14.45	49.49	34.69	22.91	98.45	0.87
	S.D.	0.70	0.52	9.12	13.36	4.24	10.44	6.55	4.17	0.34

Tab. ESM6 Physical properties of binders of mortars and binder/aggregate ratio (B/A) of mortars. The physical properties were determined indirectly using the physical properties of the mortars and composition percentages of aggregates determined by modal analysis (Table ESM2), according to the following general formula:

$X_n(B) = [X_n(M) - (X_{n(a)} \bullet \%_{(a)}) - (X_{n(b)} \bullet \%_{(b)}) - (X_{n(c)} \bullet \%_{(c)}) - (X_{n(d)} \bullet \%_{(d)}) - (X_{n(e)} \bullet \%_{(e)}) - (X_{n(f)} \bullet \%_{(f)})] / \%(A)$

Abbreviations: S.D. = standard deviation; X = physical properties; (M) = mortar; (B) = binder; (A) = aggregate; n = number from 1 to 6 of different physical properties. with X_1 = real density; X_2 = bulk density; X_3 = He open porosity; X_4 = H_2O open porosity; X_5 = He closed porosity; X_6 = imbibition coefficient; ρ_R = real density; ρ_B = bulk density; $\Phi_O He$ = helium open porosity; $\Phi_C He$ = helium closed porosity; Φ_T = total porosity; $\Phi_O H_2O$ = water open porosity; CI_W = water imbibition coefficient; SI = water saturation index; (a) = scoria; (b) = leucitite; (c) = *cocciopesto*; (d) = marble; (e) = clionpyroxene; (e) = green hornblende; (f) = biotite. The saturation index of binders is calculated as: $SI = (\Phi_O H_2O / \Phi_O He) \bullet 100$. The solid density of binder is assumed to 2.80 g/cm^3 as average of literature data

Aggregate typology	Sample	ρ_R	ρ_B	$\Phi_O He$	$\Phi_C He$	Φ_T	$\Phi_O H_2O$	CI_W	SI	B/A
		(g/cm^3)	(g/cm^3)	(%)	(%)	(%)	(%)	(%)	(%)	
Volcanic scoria aggregates	ADTH 33 b	2.40	1.46	39.28	n.d.	n.d.	38.01	26.07	96.90	n.d.
	ADTH 18 b	2.53	1.53	39.74	n.d.	n.d.	39.07	25.63	98.44	n.d.
	ADTH 50 b	2.56	1.57	38.54	n.d.	n.d.	37.93	24.18	98.55	n.d.
	ADTH 11 b	2.58	1.67	35.42	n.d.	n.d.	35.20	21.13	99.55	n.d.
	ADTH 34 b	2.56	1.63	36.27	n.d.	n.d.	36.15	22.16	99.81	n.d.
	ADTH 14 b	2.53	1.61	36.26	n.d.	n.d.	36.21	22.47	100.01	n.d.
	ADTH 12 b	2.51	1.55	38.21	n.d.	n.d.	32.46	20.69	84.96	n.d.
	Mean	2.53	1.57	37.67	n.d.	n.d.	36.43	23.19	96.89	n.d.
	S.D.	0.06	0.07	1.68	n.d.	n.d.	2.20	2.13	5.37	n.d.
Leucitite aggregates	ADTH 35 l	2.87	2.16	24.68	n.d.	n.d.	23.66	10.94	95.89	n.d.
	ADTH 58 l	2.88	2.06	28.52	n.d.	n.d.	26.11	12.66	91.57	n.d.
	ADTH 25 l	2.87	2.18	25.68	n.d.	n.d.	20.87	9.56	87.48	n.d.
	Mean	2.87	2.13	26.29	n.d.	n.d.	23.55	11.05	91.65	n.d.
	S.D.	0.01	0.06	1.99	n.d.	n.d.	2.62	1.55	4.21	n.d.
Cocciopesto aggregates	ADTH 18 c	2.85	1.58	44.49	n.d.	n.d.	38.39	24.11	86.30	n.d.
	ADTH 25 c	2.30	1.92	16.61	n.d.	n.d.	12.27	7.49	73.86	n.d.
	ADTH 3 c	2.92	1.52	47.97	n.d.	n.d.	42.52	27.82	88.65	n.d.
	ADTH 11 c	1.95	1.68	13.67	n.d.	n.d.	13.44	7.02	98.29	n.d.
	Mean	2.51	1.68	30.68	n.d.	n.d.	26.65	16.61	86.78	n.d.
	S.D.	0.46	0.17	18.04	n.d.	n.d.	16.03	10.91	10.05	n.d.

Tab. ESM7 Physical properties of aggregates and binder/aggregate ratio (B/A) of mortars.
Abbreviations: S.D. = standard deviation; ρ_R = real density; ρ_B = bulk density; $\Phi_O He$ = helium open porosity; $\Phi_C He$ = helium closed porosity; Φ_T = total porosity; $\Phi_O H_2O$ = water open porosity; CI_W = water imbibition coefficient; SI = water saturation index; n.d. = not determined

Lithoid materials	Samples	ρ_S	ρ_R	ρ_B	$\Phi_O He$	$\Phi_C He$	Φ_T	$\Phi_O H_2O$	CI_W	SI	Is_{50}	R_C	R_T
		(g/cm^3)	(g/cm^3)	(g/cm^3)	(%)	(%)	(%)	(%)	(%)	(%)	(MPa)	(MPa)	(MPa)
Lateritious 1	ADHT 41a	2.76	2.74	1.66	39.63	0.54	40.16	25.88	15.62	65.30	7.19	100.64	8.99
	ADHT 41b	2.89	2.85	1.82	36.22	1.31	37.53	29.49	16.23	81.42	7.84	109.70	9.79
	ADHT 41c	2.75	2.73	1.79	34.50	0.70	35.20	28.55	15.96	82.75	8.25	115.51	10.31
	ADHT 41d	2.88	2.84	1.84	35.06	1.38	36.44	28.06	15.22	80.03	7.91	110.73	9.89
	ADHT 41e	2.77	2.72	1.81	33.37	1.76	35.13	28.45	15.70	85.28	9.74	136.39	12.18
	Mean	2.81	2.78	1.78	35.76	1.14	36.89	28.09	15.75	78.96	8.19	114.59	10.23
	S.D.	0.07	0.06	0.07	2.40	0.51	2.08	1.34	0.38	7.87	0.95	13.32	1.19
	ADTH 2a	2.89	2.86	1.79	37.46	0.86	38.32	28.50	15.91	76.08	2.15	30.16	2.69
	ADTH 2b	2.89	2.87	1.56	45.44	0.99	46.43	24.63	15.75	54.22	3.95	55.26	4.93
	ADTH 2c	2.88	2.84	1.59	44.04	1.27	45.31	37.40	23.52	84.93	1.13	15.78	1.41
	ADTH 2d	2.94	2.88	1.62	43.75	1.80	45.56	36.93	22.76	84.40	1.17	16.32	1.46
	ADTH 2e	2.89	2.86	1.56	45.55	0.75	46.31	38.19	24.49	83.84	2.00	28.05	2.50
	Mean	2.90	2.86	1.63	43.25	1.14	44.38	33.13	20.48	76.69	2.08	29.11	2.60
	S.D.	0.02	0.02	0.10	3.33	0.42	3.42	6.16	4.29	13.08	1.14	16.03	1.43
Lateritious 2	ADGT2a	2.83	2.78	1.57	43.58	1.66	45.24	38.39	24.47	88.10	2.24	31.42	2.81
	ADGT2b	2.79	2.76	1.58	42.72	1.10	43.82	37.36	23.61	87.45	2.94	41.16	3.67
	ADGT2c	2.86	2.80	1.55	44.58	2.04	46.62	40.33	25.97	90.46	2.68	37.48	3.35
	ADGT2d	2.79	2.74	1.59	41.94	1.88	43.82	37.06	23.31	88.35	1.47	20.63	1.84
	ADGT2e	2.83	2.78	1.55	44.16	1.70	45.86	39.96	25.73	90.49	2.34	32.71	2.92
	Mean	2.82	2.77	1.57	43.40	1.68	45.07	38.62	24.62	88.97	2.33	32.68	2.92
	S.D.	0.03	0.02	0.02	1.07	0.35	1.24	1.49	1.21	1.41	0.56	7.77	0.69
Cubilia tuff	ADTH 54a	2.51	2.49	1.52	39.03	0.60	39.63	33.98	22.35	87.07	0.66	9.26	0.83
	ADTH 54b	2.47	2.45	1.52	37.92	0.75	38.67	34.28	22.54	90.39	0.47	6.65	0.59
	ADTH 54c	2.50	2.48	1.56	37.22	0.58	37.80	32.18	20.63	86.46	0.30	4.21	0.38
	ADTH 54d	2.48	2.47	1.50	39.25	0.62	39.87	35.07	23.40	89.33	1.05	14.63	1.31
	ADTH 54e	2.53	2.51	1.52	39.58	0.80	40.39	34.53	22.76	87.24	0.30	4.19	0.37
	ADTH 8a	2.44	2.44	1.53	37.34	0.28	37.61	33.08	21.67	88.61	1.04	14.49	1.29
	ADTH 8b	2.45	2.42	1.52	37.39	0.99	38.39	33.60	22.15	89.85	0.66	9.22	0.82
	ADTH 8c	2.43	2.42	1.59	34.26	0.38	34.64	31.76	19.96	92.69	0.96	13.47	1.20
	ADTH 8d	2.43	2.42	1.54	36.19	0.59	36.78	32.45	21.02	89.66	0.66	9.26	0.83
	ADTH 8e	2.43	2.41	1.55	35.99	0.65	36.63	31.46	20.34	87.42	0.97	13.59	1.21
	ADTH 23b1	2.41	2.40	1.51	37.06	0.49	37.55	30.81	20.39	83.15	0.45	6.24	0.56
	ADTH 23b2	2.44	2.42	1.48	38.81	0.92	39.73	32.19	21.77	82.94	0.38	5.28	0.47
	ADTH 23b3	2.49	2.46	1.49	39.24	1.12	40.36	31.13	20.83	79.32	0.42	5.83	0.52
	ADTH 23b4	2.41	2.39	1.45	39.43	0.61	40.04	33.84	23.32	85.82	0.85	11.92	1.06
	Mean	2.46	2.44	1.52	37.76	0.67	38.44	32.88	21.65	87.14	0.65	9.16	0.82
	S.D.	0.04	0.04	0.03	1.57	0.23	1.70	1.36	1.14	3.50	0.28	3.87	0.35
Quarry tuff	ADCA 2a	2.54	2.51	1.35	46.34	1.01	47.35	40.50	30.06	87.40	0.17	2.34	0.21
	ADCA 2b	2.55	2.52	1.32	47.54	1.02	48.55	41.77	31.55	87.87	0.19	2.62	0.23
	ADCA 2c	2.47	2.45	1.38	43.50	1.07	44.57	39.26	28.37	90.25	0.23	3.16	0.28
	ADCA 2d	2.48	2.45	1.36	44.58	1.12	45.70	41.52	30.54	93.13	0.08	1.15	0.10
	ADCA 2e	2.50	2.47	1.38	43.90	1.22	45.12	40.42	29.22	92.08	0.42	5.93	0.53
	ADCA1a	2.50	2.46	1.43	41.80	1.59	43.39	38.51	26.93	92.12	0.24	3.42	0.30
	ADCA1b	2.46	2.44	1.43	41.49	0.93	42.42	39.06	27.38	94.15	0.15	2.06	0.18
	ADCA1c	2.45	2.43	1.41	41.75	0.92	42.67	39.63	28.04	94.91	0.24	3.35	0.30
	ADCA1d	2.48	2.45	1.43	41.85	1.16	43.01	38.28	26.83	91.48	0.15	2.08	0.19
	Mean	2.49	2.46	1.39	43.64	1.12	44.75	39.88	28.77	91.49	0.21	2.90	0.26
	S.D.	0.03	0.03	0.04	2.19	0.20	2.15	1.25	1.68	2.59	0.10	1.35	0.12

Tab. ESM8 Physical data determined on 15 specimens of 3 samples of *lateritious* (ADTH 2, ADTH 41 from *Heliocaminus* Baths and ADGT2 from "Grandi terme" Baths of Hadrian Villa), 14 specimens of 3 samples of *cubilia* tuff (ADTH 54, ADTH 8, ADTH 23) and 9 specimens of 2 samples from quarry tuff (ADCA 2, ADCA 1)

Abbreviations: S.D. = standard deviation; ρ_R = real density; ρ_B = bulk density; $\Phi_O He$ = helium open porosity; $\Phi_C He$ = helium closed porosity; Φ_T = total porosity; $\Phi_O H_2O$ = water open porosity; CI_W = water imbibition coefficient; SI = water saturation index; Is_{50} = Point Load strength index; R_C = compression strength; R_T = tensile strength